MISCELLANEOUS PAPER GL-89-16

SPECTRAL CHARACTERISTICS OF SMALL MAGNITUDE EARTHQUAKES WITH APPLICATION TO WESTERN AND EASTERN NORTH AMERICAN TECTONIC ENVIRONMENTS: SURFACE MOTIONS AND DEPTH EFFECTS

by

Robert B. Darragh, Robert K. Green, F. Thomas Tarcotte

Woodward-Clyde Consultants
500 12th Street, Suite 100
Oakland, California 94607-4014

September 1989
Final Report

Prepared for DEPARTMENT OF THE ARMY
US Army Corps of Engineers
Washington, DC 20314-1000

Under Contract No. DACW39-88-M-0146

Monitored by Geotechnical Laboratory
US Army Engineer Waterways Experiment Station
3909 Halls Ferry Road
Vicksburg, Mississippi 39180-6199

REPORT DOCUMENTATION PAGE

Form Approved OMB No. 0704-0188

1a REPORT SECURITY CLASSIFICATION Unclassified	1b RESTRICTIVE MARKINGS
2a SECURITY CLASSIFICATION AUTHORITY	3 DISTRIBUTION/AVAILABILITY OF REPORT Approved for public release; distribution unlimited.
2b DECLASSIFICATION/DOWNGRADING SCHEDULE	
4 PERFORMING ORGANIZATION REPORT NUMBER(S)	5 MONITORING ORGANIZATION REPORT NUMBER(S) Miscellaneous Paper GL-89-16
6a NAME OF PERFORMING ORGANIZATION Woodward-Clyde Consultants 6b OFFICE SYMBOL (If applicable)	7a NAME OF MONITORING ORGANIZATION Geotechnical Laboratory USAEWES
6c ADDRESS (City, State, and ZIP Code) 500 12th Street, Suite 100 Oakland, CA 94607-4014	7b ADDRESS (City, State, and ZIP Code) 3909 Halls Ferry Road Vicksburg, MS 39180-6199
8a NAME OF FUNDING/SPONSORING ORGANIZATION US Army Corps of Engineers 8b OFFICE SYMBOL (If applicable)	9 PROCUREMENT INSTRUMENT IDENTIFICATION NUMBER Contract No. DACW39-88-M-0146
8c ADDRESS (City, State, and ZIP Code) Washington, DC 20314-1000	10 SOURCE OF FUNDING NUMBERS PROGRAM ELEMENT NO. / PROJECT NO. / TASK NO. / WORK UNIT ACCESSION NO

11 TITLE (Include Security Classification) Spectral Characteristics of Small Magnitude Earthquakes with Application to Western and Eastern North American Tectonic Environments: Surface Motions and Depth Effects

12 PERSONAL AUTHOR(S)
Darragh, Robert B.; Green, Robert K.; Turcotte, F. Thomas

13a TYPE OF REPORT	13b TIME COVERED	14 DATE OF REPORT (Year, Month, Day)	15 PAGE COUNT
Final report	FROM _____ TO _____	September 1989	89

16 SUPPLEMENTARY NOTATION
Available from National Technical Information Service, 5285 Port Royal Road, Springfield, VA 22161.

17 COSATI CODES			18 SUBJECT TERMS (Continue on reverse if necessary and identify by block number)
FIELD	GROUP	SUB-GROUP	Earthquakes Ground motions Response spectra

19 ABSTRACT (Continue on reverse if necessary and identify by block number)

The band-limited-white-noise model employed in the WES-RASCAL computer program has been used to predict response spectral shapes for small magnitude earthquakes (moment magnitude (M_w) ≈ 5.3 to 2.5) in both eastern and western North America. Model predictions are compared to spectral shapes computed from data recorded in both eastern North America (ENA) and western North America (WNA) tectonic provinces. The ground motion model produces reliable and accurate predictions of spectral composition as well as peak accelerations for these small magnitude earthquakes. Results of magnitude and distance scaling of response spectral shapes show little distance dependence in the range of 5 to 25 km, but a strong magnitude dependence in the range M_w 2.5 to 5.3.

Representative synthetic acceleration time histories have also been generated at close ranges for rock outcrops with properties typical of WNA and ENA. The synthetic motions compare favorably in peak acceleration, duration, and spectral content (Continued)

20 DISTRIBUTION/AVAILABILITY OF ABSTRACT	21 ABSTRACT SECURITY CLASSIFICATION
☒ UNCLASSIFIED/UNLIMITED ☐ SAME AS RPT ☐ DTIC USERS	Unclassified
22a NAME OF RESPONSIBLE INDIVIDUAL	22b TELEPHONE (Include Area Code) / 22c OFFICE SYMBOL

19. ABSTRACT (Continued).

with recorded data at comparable magnitudes and ranges.

Ground motions are also examined at depths of 50, 100, and 150 m within a half-space. The effects of depth upon response spectra, Fourier spectra, peak acceleration, and peak particle velocity are shown. Depth-dependent spectral nodes are present in the Fourier and response spectra. Both peak acceleration and peak particle velocity decrease with depth. Peak acceleration decreases more rapidly with depth than does peak particle velocity.

PREFACE

This report was prepared by Dr. Robert B. Darragh under the direction of Dr. Walter J. Silva under Contract No. DACW39-88-M-0146. Mr. Robert K. Green and Dr. F. Thomas Turcotte contributed to the study. Time histories from the Anza array were made available by the Institute of Geophysics and Planetary Physics of the University of California, San Diego. Time histories from the aftershocks of the Painesville, Ohio, earthquake were made available by Dr. Roger Borcherdt of the US Geological Survey, Menlo Park, California.

This study was performed under the supervision of Dr. Ellis L. Krinitzsky, Earthquake Engineering and Geosciences Division (EEGD), Geotechnical Laboratory (GL), US Army Engineer Waterways Experiment Station (WES). The work is part of an ongoing investigation in the Civil Works R&D Program, Earthquake Hazard Evaluations for Engineering Sites. General supervision was provided by Dr. A. G. Franklin, Chief, EEGD, and Dr. W. F. Marcuson III, Chief, GL.

COL Larry B. Fulton, EN, is Commander and Director of WES. Dr. Robert W. Whalin is Technical Director.

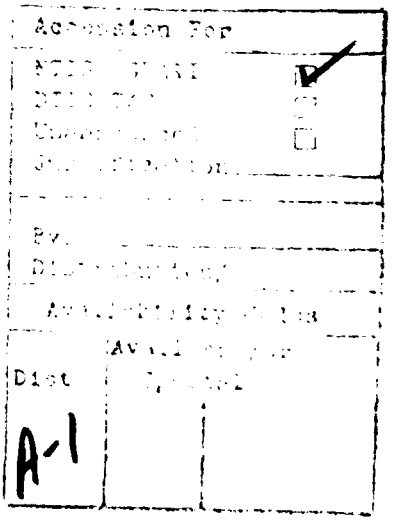

TABLE OF CONTENTS

SPECTRAL CHARACTERISTICS OF SMALL MAGNITUDE EARTHQUAKES WITH APPLICATION TO WESTERN AND EASTERN NORTH AMERICAN TECTONIC ENVIRONMENTS: SURFACE MOTIONS AND DEPTH EFFECTS

PART I: INTRODUCTION

Purpose

1. The purpose of this study is to characterize, in western (WNA) and eastern (ENA) North American tectonic environments, response spectral shapes (five percent response spectral acceleration divided by peak acceleration) and acceleration time histories expected from small magnitude earthquakes recorded at close distances on competent rock. The moment magnitude (M_w) range is approximately 2.0 to 5.3. Competent rock is defined, for purposes of this study, as rock with a shear wave velocity of 3.2 km/sec and 3.5 km/sec in WNA and ENA, respectively.

2. This study will document the differences in spectral shape and acceleration time histories in WNA and ENA by examining recorded data in three moment magnitude ranges: approximately $2.0 \leq M_w \leq 2.5$, $4.0 \leq M_w \leq 4.9$, and $5.0 \leq M_w \leq 5.6$. These differences will be modeled with a band-limited-white-noise (BLWN) ground motion model described below. The BLWN model will be shown to be able to reliably predict spectral shapes for WNA and ENA tectonic environments for these magnitude ranges, as well as produce realistic acceleration time histories.

3. In addition, the effects of receiver depths will be examined using the BLWN model. Fourier spectra are produced for depths of 50, 100, and 150 m within a homogenous rock half-space. Random vibration theory (RVT) is used to predict response spectral ordinates as well as peak acceleration and peak particle velocity at these depths.

4. It is important to state that the results of this study are intended to demonstrate the predictions using a single analysis method, and are not intended for use in the design of specific structures.

Method

5. The estimates of the ground motion parameters are made using a band-limited-white-noise (BLWN) ground motion model as described by Boore and Atkinson (1987). This model uses the stochastic, constant stress parameter ground motion model (Hanks, 1979; McGuire and Hanks, 1980; Hanks and McGuire, 1981; Boore, 1983, 1986a; McGuire et al, 1984; Atkinson, 1984; and Boore and Atkinson, 1987) coupled with a simple single corner frequency - omega square source model (Brune, 1970, 1971). Random vibration theory is used to relate the root mean square (RMS) values of acceleration and velocity, as well as, oscillator response computed from the power spectra to the corresponding expected peak time domain values. The ground motion model is described in more detail in Part III.

6. Representative acceleration time histories are developed using a method presented in Silva and Lee (1987). This method involves combining the Fourier amplitude spectrum from the BLWN model with the phase spectrum of a recorded accelerogram to produce a synthetic time history. This method is described in more detail in Part IV.

PART II: SPECTRAL DIFFERENCES IN OBSERVED DATA

7. Strong ground motion observed at rock sites in eastern North America appears to have different spectral properties than those typical of western North America rock sites. These differences are demonstrated by comparing the response spectral shapes and acceleration time histories from WNA and ENA tectonic environments for similar ranges and moment magnitudes.

8. In selecting the data as representative of ENA and WNA rock sites, an attempt was made to use only those sites which are composed of competent rock. For this study, rock is defined as material with a shear-wave velocity exceeding approximately 760 m/sec (2500 ft/sec). Possible exceptions to the criterion include the New Hamphire (1982) earthquake recordings upon earth dams, and the Painesville, Ohio (1986) aftershocks recordings upon stiff soil (till) (Borcherdt, 1986). Sites founded upon very thin alluvium sections (<5m), such as some of the recordings of the New Brunswick (1982) sequence, are also used since any resonance phenomena will be at high frequencies and, as such, not perturb the spectral shapes to a great degree.

Ground Motions Recorded in WNA

9. The recorded ground accelerations used in this study are listed in Tables 3, 5, and 7 for M_w approximately 5.3, 4.5, and 2.5, respectively. For M_w = 5.3 (Table 3), the acceleration data were recorded during the 1970 Lytle Creek, California earthquake and aftershocks of the 1983 Coalinga, California earthquake. In general, these accelerograms were recorded on SMA-1 instruments. The Nyquist frequency of the processed data is 25 Hz. The processing has followed the standard techniques used by California Institute of Technology, California Division of Mines and Geology (CDMG), or the U.S. Geological Survey (USGS). All the recording sites are classified as either sedimentary or crystalline rock.

10. For M_w = 4.5 analysis (Table 5) the acceleration data were recorded during the 1971 Oroville, California earthquake sequence. These time histories were recorded on SMA-1 instruments at sites located on crystalline rock. The Nyquist frequency of the processed data is 100 Hz. The accelerograms were recorded by CDMG and processed by Woodward-Clyde Consultants using standard processing with a time step of 0.005 seconds.

11. The Anza, California array data (Table 7) were recorded digitally with velocity instruments with a sample rate of 250 samples/sec and a dynamic range of 96 db. The two stations chosen (PFO and KNO) are sited on crystalline rock within the Southern California batholith. The Anza array is described in detail in Berger et al (1984).

Ground Motions Recorded in ENA

12. The recorded ground accelerations used in this study are listed in Tables 4, 6, and 8 for M_w approximately 5.3, 4.5, and 2.5, respectively. For M_w = 5.3 (Table 4) two aftershocks of the 1985 Nahanni, Canada earthquake were selected. The thrust mechanisms, regional stress regime, shallow focal depth, and high velocity sedimentary rocks in the focal region suggest that the near-source strong ground motions recorded are applicable to ENA (Wetmiller et al., 1988). The recording instruments are SMA-1 with corner frequencies near 25 Hz and the processed data have a sample rate of 200 samples/sec with the corresponding Nyquist frequency of 100 Hz (Wiechert et al., 1986).

13. Accelerograms produced by aftershocks of three earthquakes were chosen for the M_w = 4.5 analysis (Table 6). These records were generally recorded by SMA-1 instruments and sampled at rates of 200 samples/sec and higher. The instruments were sited on sedimentary or crystalline rocks for the New Brunswick and Nahanni aftershocks. For the

1982 New Hampshire earthquake, the instruments were sited on or near two dams (Chang, 1983). Correction procedures for these data follows those of the USGS at Menlo Park.

14. For the M_w = 2.5 analysis (Table 8), two aftershocks of the 1986 Painesville, Ohio earthquake recorded on till were selected. The recordings were made by the General Earthquake Observatory System (GEOS) employing velocity instruments. A sampling rate of 400 samples/sec was used and no anti-alias filters were applied (Borcherdt, 1986).

Response Spectral Shapes

15. The difference in spectral content can perhaps be most easily appreciated in spectral amplification (Sa/a) computed from recordings typical of WNA and ENA tectonic environments. Figure 1 shows average response spectral shapes computed from recordings made on rock of the 1985 Nahanni aftershocks ($M_w \approx 5.3$, Table 4) compared to an average spectral shape computed from $M_w \approx 5.3$ WNA rock motions (Table 3). The differences in spectral content appear significant and indicate that, for the same level of peak acceleration, ENA spectral content may be higher than that in the WNA for frequencies greater than approximately 10 Hz.

16. Figure 2 shows the average response spectral shape computed from recordings made on crystalline rock of the 1971 Oroville aftershocks ($M_w \approx 4.5$, Table 5) compared to an average spectral shape computed from earthquakes in New Brunswick, New Hampshire, and Nahanni ($M_w \approx 4.5$, Table 6). The differences in spectral content appear to be significantly less than those exhibited in the previous $M_w \approx 5.3$ comparison. The shifting of the frequency of maximum spectral amplification from approximately 7 Hz for the WNA M_w 5.3 to 13 Hz for the M_w 4.5 may be related to the differences in recording site conditions. The Oroville data are representative of sites located on hard crystalline rock (Hanks, 1982) while the corresponding sites for the M_w = 5.3 data are comprised generally of softer

sedimentary rocks. The differences in the upper crustal rocks would be reflected in markedly different values for kappa or f_{max} (Boore and Atkinson, 1987; Hough and Anderson, 1988) which, in the BLWN ground motion model, control the short-period portion of the response spectra (Silva and Green, 1988).

17. An additional factor which complicates the comparison at short periods is the effect of processing, specifically low pass filtering, upon response spectra. For ENA accelerograph data, due to generally higher frequency content, sample rates are at least 200 samples/sec and anti-alias filters normally employ a cosine bell from 50 to 100 Hz. This gives an effective bandwidth from several seconds (depending upon magnitude) to 50 Hz provided one is willing to accept the accuracy of the instrument correction beyond the corner frequency of the transducer (25 Hz in the SMA-1). For WNA data, the sample rate may be as low as 50 samples/sec with anti-alias filters applied at 23 Hz. The effective bandwidth then becomes from several seconds to 23 Hz. While this bandwidth is generally sufficient for most WNA strong motion data, it may be too narrow for recording instruments founded upon hard crystalline rock outcrops (see Anza array data discussion). This band limitation may be a contributing factor limiting the short-period response of the Oroville data. Further, it suggests that the differences at high frequencies in response spectral shapes between ENA and WNA tectonic environments may be largely confined to differences in the shallow crust.

18. Figure 3 shows average response spectral shapes computed from recordings of three 1982 Anza ($M_w \approx 2.5$) earthquakes (Table 7) compared to an average spectral shape computed from recordings of aftershocks of the Painesville, Ohio earthquake (Table 8). In this case, the spectral composition appears to be nearly the same for both ENA and WNA motion. For both spectrums, the period of maximum amplification occurs at approximately 0.03 seconds and the shapes are nearly identical for periods longer than 0.1 seconds. The similarity in shape is probably a consequence of very

similar average shear-wave damping as well as velocity in the upper few km of the crust. The two Anza stations are founded upon hard rock with low values of kappa (Hough and Anderson, 1988) relative to kappa values appropriate for softer, more typical WNA, rock sites (Anderson and Hough, 1984). Conversely, the site which recorded the Painesville aftershock were founded upon stiff soil (till) and may reflect a somewhat lower value of kappa than is appropriate for hard ENA rock conditions.

19. The similarity in response spectral shapes shown in Figure 3 certainly implies a similarity in Fourier spectral densities and may suggest similar stress drops for these events. However, due to the possible effects of resonances, as well as damping, which may bias the interpretation of Fourier amplitude spectra in terms of source properties, it is difficult to compare detailed analysis of data recorded at shallow soil sites with analyses from data recorded at competent rock outcrops (Cranswick et al., 1985).

Acceleration Time Histories

20. In order to demonstrate differences and similarities in spectral content in the time domain, Figures 4, 5, and 6 show representative time histories recorded in WNA for $M_w \approx 5.3$, 4.5, and 2.5 earthquakes respectively as well as representative ground acceleration time histories recorded in ENA for $M_w \approx 5.3$, 4.5, and 2.5 events respectively. The large difference in spectral content for the $M_w \approx 5.3$ comparison is evident in Figure 6. Figure 5, the $M_w \approx 4.5$ comparison, shows some differences in spectral content with the ENA motions possessing more energy at high frequencies. Finally, the $M_w \approx 2.5$ comparison in Figure 6 shows comparable frequency content between a time history recorded at the Anza, California array and one recorded in Painesville, Ohio.

21. Other studies and sources of data also indicate a consistency in high frequency spectral content of ENA recordings made upon rock or stiff soil sites. These include aftershocks of the 1982 Miramichi, New Brunswick event (Cranswick et al., 1985), the 1982 Enola, Arkansas swarm (Haar, et al 1984), and the 1986 Painesville, Ohio event (Wesson and Nicholson, 1986) and its aftershocks (Borcherdt, 1986; Borcherdt and Glassmoyer, 1987).

22. The trends shown in the response spectral shapes and reflected in the time histories suggest that a controlling factor of strong ground motion at high frequencies is associated with the rock quality in the upper crust. This observation is consistent with that of Anderson and Hough (1984) and Hough and Anderson (1988) who parameterized this effect in terms of the distance dependent exponential damping factor called kappa. They attribute the positive value of kappa at zero distance to damping in the upper 2-5 km of the crust.

23. In the following sections, the differences in response spectral shapes computed from observed data will be interpreted in terms of the band-limited-white-noise ground motion model. In this model, the magnitude dependence of the spectral shapes is controlled by the single-corner-frequency Brune (1970, 1971) source spectrum. The high frequency fall-off (Hanks, 1982) will be modeled using the Anderson - Hough kappa operator. It is important to emphasize that we are not attempting to perform detailed source or path modeling in this study. We are simply illustrating the effectiveness of a simple, physically based, and computationally straightforward ground motion model to capture the essential elements, on an average basis, of strong ground motion for engineering purposes.

PART III: GROUND MOTION MODEL

24. The BLWN ground motion model in which the energy is distributed randomly over the duration of the source has proven remarkably effective in correlating with a wide range of ground motion observations (Toro, 1985; Boore, 1986a). Time-domain measures such as peak acceleration and peak velocity, Wood-Anderson magnitude, and short-period P- and S-wave amplitudes, as well as, frequency domain measures such as, relative velocity response and Fourier amplitude spectra have been predicted with reasonable accuracy using the stochastic (BLWN) ground motion model (Boore, 1983; McGuire et al., 1984; Boore, 1986a; Boore and Atkinson, 1987; Toro and McGuire, 1987). The stochastic ground motion model employed here uses an ω-square source model (Brune; 1970, 1971) with a single corner frequency and a constant-stress-parameter (Boore, 1983; Atkinson, 1984). Random vibration theory is used to relate RMS values to peak values of acceleration (Boore, 1983), and oscillator response (Boore and Joyner, 1984; Toro, 1985; Silva and Lee, 1987) computed from the power spectra to expected peak time domain values (Boore, 1983).

25. The shape of the acceleration spectral density a(f) is given by

$$a(f) = C \frac{f^2}{1+(f/f_c)^2} \frac{M_o}{R} P(f) A(f) e^{-\frac{\pi f R}{\beta Q(f)}}$$

where C = constant which contains source region density and shear-wave velocity terms and accounts for the free-surface effect, the source radiation pattern, and the partition of energy into two horizontal components.

M_o = seismic moment,

R = hypocentral range,

β = shear wave velocity at the source,

$Q(f)$ = frequency dependent quality factor,

$A(f)$ = near-surface amplification factors (Boore, 1986a),

$P(f)$ = high-frequency truncation filter, and

f_c = source corner frequency.

26. Source scaling is provided by specifying two independent parameters, taken to be seismic moment (M_o) and the high-frequency stress parameter ($\Delta\sigma$). The moment is related to magnitude through the definition of moment magnitude M_w, by the relation:

$$\log M_o = 1.5\ M_w + 16.1 \qquad \text{(Hanks and Kanamori, 1979)},$$

27. The stress parameter, $\Delta\sigma$ is assumed to be independent of magnitude and is taken to be 50 bars in WNA (Boore, 1986a) and 100 bars in ENA (Toro, 1985; Boore and Atkinson, 1987). The Q(f) models are shown in Table 1 along with the remaining parameters considered to be representative of the WNA and ENA tectonic environments. The near-surface amplification factors (Table 2), that account for the increase in amplitude as the seismic energy travels through lower velocity crustal materials near the surface, are taken from Boore (1986a). Because the near-surface (upper crustal) velocity gradients are smaller in the central and eastern tectonic environments, the factors are applied only in the WNA simulations (Boore and Atkinson, 1987).

28. The Fourier amplitude spectrum given by the equation for a(f) represents the BLWN ground motion model employing a Brune source spectrum that is characterized by a single corner frequency. In order to compute peak time domain values, that is, peak acceleration and peak oscillator

response, random vibration theory (RVT is used to relate RMS computations to peak value estimates. Boore (1983) and Boore and Joyner (1984) contain an excellent development of the RVT methodology as applied to the BLWN ground motion model. The procedure, in general, involves computing the RMS value by integrating the power spectrum from zero frequency to the Nyquist frequency and applying Parsevall's relation. Extreme value theory is then used to estimate the expected ratio of the peak value to the RMS value of a specified duration of the BLWN time-history. The duration is generally taken as the inverse of the corner frequency (Boore, 1983).

29. The P(f) filter is an attempt to model the observation that acceleration spectral density appears to fall off rapidly beyond some region-dependent maximum frequency. This observed phenomenon truncates the high frequency portion of the spectrum and is responsible for the band-limited nature of the stochastic model. This spectral fall off has been attributed to near-site attenuation (Hanks, 1982; Anderson and Hough, 1984) or to source processes (Papageorgiou and Aki, 1983) or perhaps to both effects. Two forms have been proposed for this filter: (1) an acausal four-pole, low-pass Butterworth filter with a corner frequency given by Hanks' site-dependent f_{max} (Boore, 1983), and (2) a site and distance dependent exponential filter proposed by Anderson and Hough (1984). The form of the Butterworth filter is given by:

$$P(f) = [1 + (f/f_m)^8]^{-1/2}$$

where f_m is taken as f_{max} (Hanks, 1982; Boore, 1983; 1986a).

30. The other form of the P(f) filter, the exponential filter, is given by

$$P(f) = e^{-\pi\kappa f}$$

where kappa (κ) is a site and distance dependent parameter that represents the effect of intrinsic attenuation on a wavefield propagating through the upper crust. Kappa has been determined for several rock and soil sites representative of western North America (Anderson and Hough, 1984; Anderson, 1986a). For WNA rock sites, a value near 0.02 sec is appropriate (Boore, personal communication, 1988). For eastern North America, the relationship kappa = $\frac{1}{\pi f_{max}}$ may be used to infer a kappa 0.008 sec consistent with an ENA f_{max} of 40 Hz (Boore and Atkinson, 1987). This relationship produces response spectra which have peak spectral amplification near the same period for P(f) modeled by kappa or f_{max}. The relationship kappa = $\frac{1}{2\pi f_{max}}$ results in a kappa of 0.004 sec for an f_{max} of 40Hz. For this relationship, the RMS values are nearly equal (Toro, personal communication, 1988). For this study kappa = 0.006 sec was used in the generation of artificial motion for ENA as well as in the section on motion at-depth. In the comparisons of predicted spectral shapes to average spectral shapes computed from observed data, kappa values which provided the best fit were used if the average shape was computed from stations founded on similar rock type (hard or soft). Otherwise the standard values of 0.02 sec and 0.006 sec (Table 1) were used to compute shapes for WNA and ENA, respectively.

PART IV: GENERATION OF SYNTHETIC ACCELERATION TIME HISTORIES

Description of the Technique

31. Synthetic time histories can be generated using a method based upon the ability of the BLWN model, with a simple ω-square constant-stress-parameter source, to successfully predict a variety of measures of ground motion over a wide magnitude and distance range. Implied in this success is that the general shape of the BLWN spectrum is an adequate representation, in many circumstances, of the physical process actually occurring in the earth. If one can assume that over the period range of engineering interest to critical facilities, 3 seconds to approximately 25 Hz, a critical facility cannot discriminate the Fourier amplitude spectrum between: 1) a simple point source approximation, instantaneous rupture over a circular fault zone and wave propagation in a uniform half-space; and 2) and a more rigorous representation of the earthquake source and wave propagation phenomena, then much of the difference may be contained in the Fourier phase spectrum. This is not an unreasonable assumption as the Fourier phase spectrum determines the distribution of energy in time and, as such, contains information regarding source, path, and site effects.

32. The technique of combining the Fourier phase spectrum from an observed strong motion record with the BLWN amplitude spectrum has been used to generate realistic time histories for a variety of source, path, and site conditions (Silva and Lee, 1987; Norm Abrahamson, personal communication, 1988). In general, the results produced not only realistic acceleration time histories, but also integrations to velocity and displacement that appear indistinguishable from observed records as well. In order to produce synthetic records which have appropriate duration characteristics, the phase should be extracted from records of earthquakes with magnitudes within 1/2 unit of the design event (Silva and Lee, 1987). A suite of time histories may be quickly generated by combining different phases with the same amplitude spectrum. Analyses performed with these

time histories then impart the same spectral distribution of power into a system, but the distribution of levels of excitation in time will naturally differ for each input accelerogram.

33. As an example, local synthetic time histories are generated by combining the Fourier phase spectrum from a WNA strong motion record with the BLWN amplitude spectrum using either WNA or ENA source and propagation path operators (Table 1). While a phase spectrum from a WNA recording may not be appropriate for use in the context of an ENA tectonic environment (and vice-versa), the assumption is that if any differences exist, they may be significant only at high frequencies beyond 20 Hz. The use of a Fourier phase spectrum from WNA recordings to generate ENA ground motions allows a much greater range in magnitudes as well as distances thereby increasing the flexability of the technique. At distances where the predominant motion is generated by phases (such as Lg) which do not propagate well in WNA, this assumption is of course not valid. Additionally, due to differences in crustal structure between WNA and ENA, circumstances exist where the simple BLWN model may not produce an adequate Fourier amplitude spectrum (Burger et al., 1987).

34. In order to emulate the effects of filtering in the processing of the strong motion recordings, five-pole causal Butterworth filters are applied to the synthetic time histories in the frequency domain. For the M_W = 5.3 and 4.5 synthetic time histories, low-pass filters with corners at 23 Hz and 75 Hz are applied for the WNA and ENA motions respectively. For the M_W = 2.5 time history, no filters were applied for ENA, while the WNA synthetics were low-pass filtered with a six-pole at 62.5 Hz (the corner frequency of the anti-alias filters).

Examples of the Technique

35. Figures 7, 9, and 11 display synthetic and observed accelerograms for eastern North American rock sites for moment magnitudes 5.3, 4.5, and 2.5 respectively. Accelerogram No. 1 (top time history) in each figure has been generated, as described earlier, by combining the phase spectrum from a recorded WNA accelerogram with the appropriate BLWN amplitude spectrum. Accelerograms No. 2 and No. 3 are observed ground motions near the appropriate magnitude and distance range in the eastern United States. In each figure, the synthetic acceleration time history appears realistic with reasonable values of maximum acceleration, duration, and distribution of energy in time. Also, the synthetic acceleration time history displays the typical non-stationarity contained in the observed ground motions. Figures 8, 10, and 12 are the 5% response spectral shapes for the synthetic and observed accelerograms shown in Figures 7, 9, and 11, respectively. Also, on each of these three figures the WES-RASCAL RVT estimate of the 5% response spectral shape is plotted. The RVT response spectral shape is smooth. The observed response spectral shapes as well as the response spectral shape computed from the synthetic acceleration time history show characteristic peaks and valleys. In all three cases, the 5% response spectral shape generated by the method described above appears reasonable.

36. To demonstrate the synthesis method at closer ranges, accelerograms are generated at a hypocentral range of 10 km for moment magnitudes 3.0, 4.0, and 5.0 for both WNA and ENA using the standard parameters shown in Table 1. The results for ENA are shown in Figure 14. As expected, the acceleration time history displays more energy at higher frequencies than present in the WNA synthetic (Figure 13) which is due to the different value used for kappa (Table 1). The peak accelerations in Figure 14 are larger than the corresponding WNA peak accelerations in Figure 13.

37. Figure 15a shows the WES-RASCAL peak acceleration magnitude scaling for WNA at a distance of 10 km over the M_w range of 2.0 to 8.0. Also shown are two WNA empirical relationships plotted over the magnitude range for which the relationships are constrained by data. The long-dashed line represents the Joyner-Boore (Joyner and Fumal, 1985) relationship and the short-dashed line represents Campbell (1985) relationship for hard rock. Considering the statistical variability associated with the empirical estimates, the agreement between the model predictions and those of the empirical relationships are reasonably good over the M_w range of approximately 3 to 7.5. Below $M_w \approx 3$, the BLWN RVT predictions drop below those of Campbell (1985). At $M_w \approx 2.5$ the BLWN RVT prediction is below Campbell (1985) by a factor of 2. It is difficult to assess the significance of this departure at these small magnitudes in view of the amount of data actually constraining the empirical relationship. The predicted peak acceleration for a $M_w \approx 2.5$ at 10 km is about 10^{-2} g which is at the nominal threshold of an SMA-1 accelerograph. As a consequence, strong ground motion recordings in this magnitude and distance range may be biased by recordings at sites which tend to amplify ground motions.

38. A similar comparison for ENA is shown in Figure 15b. On this Figure 15, the BLMW RVT predictions are compared to Toro and McGuire (1987), Boore and Atkinson (1987), and to a Nuttli semi-empirical relationship for South Carolina (Nuttli et al., 1986). This latter relationship was used as it was thought to be more appropriate for rock sites. The Toro and McGuire (1987) and Boore and Atkinson (1987) relationships are derived from a regression upon BLWN RVT predictions for ENA. The relationship

$$M_w \approx 2.715 - 0.277\ m_{Lg} + 0.127\ m_{Lg}^2 \qquad \text{(Boore and Atkinson, 1987)}$$

has been used to relate m_{Lg} to M_w in the Nuttli (Nuttli et al., 1986) and Toro and McGuire (1987) prediction equations. The general agreement between the RVT based predictions is not surprising since all are fundamentally similar and use nearly the same parameter values. The Nuttli (Nuttli et al., 1986) relationship falls below RVT based predictions for magnitudes less than 5-6. In view of the limited data base with which to constrain the relationship, such departures are not unexpected.

PART V: COMPARISON OF MODEL PREDICTIONS WITH OBSERVED DATA

Western North American Comparison

39. As a consequence of the differences in earthquake recurrence between WNA and ENA, the comparisons between model predictions and observations for ENA are few in number compared to the WNA. However, it should be noted that free field recordings on competent rock, properly sampled and processed, for magnitudes (M_w) below about 4.0 form a sparse data set in both ENA and WNA.

40. For the WNA comparative analysis, predicted 5% response spectral shapes computed using WNA parameters (Table 1) for M_w 5.3, 4.5, and 2.5 at a distance of 25 km are compared to spectral shapes computed from recordings at a variety of rock sites. The earthquakes used have local magnitudes (M_L) at or near the values of M_w given above. The epicentral distances are all within 50 km. For each magnitude comparison, the events and stations used, M_L, distance and hypocentral depth, when available, and the average horizontal peak acceleration are listed in Tables 3, 5, and 7.

41. In computing the 5% response spectral shapes from the recorded data, the absolute acceleration response spectrum (5% damping) is computed from each component and then normalized by the peak acceleration of that component. The spectral shape for each magnitude classification is then computed as a simple arithmetic average at each period. In Figures 16 through 21, the dotted lines represent the upper and lower bounds of the set of spectral shapes used in computing the average. Therefore, contributions to the bounds generally come from several or all of the shapes at different periods and reflect the absolute dispersion of the data.

42. Figure 16 shows the M_w = 5.3 comparison of the WES-RASCAL predicted spectral shape with the spectral shape computed from the data listed in Table 3. The recordings from six earthquakes were available for analysis: 1970 Lytle Creek (M_L = 5.4), and five aftershocks of the 1983 Coalinga earthquake. This represents a fairly homogeneous data set in terms of weight of one site (10 components from the Coalinga site Baths) and the fit of the WES-RASCAL model to the data is quite good. A kappa of 0.03 sec was found to be suitable for these soft rock sites which may be most appropriate for the Baths site.

43. The comparison at magnitude, M_w = 4.5, is shown in Figure 17. The average spectral shape was computed from aftershocks of the 1975 Oroville earthquake (Table 5). M_L ranged from 4.0 to 4.9 and the BLWN model was computed for an M_w = 4.5 earthquake at a hypocentral range of 25 km. The sites chosen (6, 8, 9) were located on crystalline rock with an estimated representative f_{max} of 20 Hz (Hanks, 1982). The standard value of 0.02 sec (Table 1) was used for kappa in the model. Although the range in M_L and source depth is large, this data set reflects the most homogeneous set of site conditions, and the fit is certainly good.

44. Figure 18 shows the comparison for M_w = 2.5. This data set consists of three microearthquakes recorded at two stations in the Anza array (PFO and KNW, Table 1). A kappa of 0.009 sec is used in the model predictions. The fit is reasonably good up to approximately 10 Hz. Between 10 Hz and 20 Hz the model underpredicts the average spectrum computed from the rock readings. However, this part of the spectrum may have been biased upward by the presence of a possible site resonance which shows in the envelope at a period of 0.08 seconds.

Eastern North America Comparison

45. As alluded to in the previous section, the comparison to ENA spectral shapes is tenuous at best due to the paucity of data particularly for magnitudes (m_{Lg}) other than approximately 5.

46. For the ENA comparative analysis, predicted spectral shapes computed using ENA parameters (Table 1) for moment magnitudes 5.3, 4.5 and 2.5 at a distance of 25 km are compared to spectral shapes computed from recordings at a variety of rock sites, earth dam sites, and two stiff soil sites. The earthquakes used have magnitudes (m_b, m_{Lg}, or M_{coda}) at or near the moment magnitudes given above. The epicentral distances are nearly all within 50 km. For each magnitude comparison, the events and stations used, magnitude, distance and depth when available, and the average horizontal peak acceleration are listed in Tables 4, 6 and 8.

47. Figure 19 shows the M_w = 5.3 comparison with the data listed in Table 4. The recordings from two aftershocks of the 1985 Nahanni mainshock were available for analysis. The standard kappa of 0.006 sec was found to be appropriate for these rock sites. The departure of the predicted spectral shape using a kappa of 0.006 sec from the trend shown by the data beyond about 20 Hz suggests a departure from model predictions. However, this overprediction may be an artifact of the recording since the strong motion instruments (SMA-1) all had corner frequencies near 25 Hz. While instrument corrections were performed (Wiechert et al., 1986), it is notoriously difficult to correct with confidence through an instrument corner unless very accurate phase and amplitude calibrations are available. Thus, confidence in the data should not be particularly high for frequencies exceeding 20 to 25 Hz. The kappa operator appears to give a reasonable representation of the spectral shape computed from recorded data over the bandwidth of interest (1 to 25 Hz) to critical structure.

48. The comparison at magnitude, M_w = 4.5, is shown in Figure 20. The average spectral shape was computed from aftershocks of three ENA earthquakes (Table 6). Magnitudes ranged from 4.0 to 4.8 and the BLWN model was computed for an M_w = 4.5 earthquake at a hypocentral range of 8 km. A kappa of 0.006 sec provided the best fit and was used in the model. The fit is good from 100 Hz to around 1 Hz.

49. Figure 21 shows the comparison for M_w = 2.5. The average spectral shape was computed from two aftershocks recorded at two stiff soil sites (till) of the 1986 Painesville, Ohio earthquake (Table 8). The predicted shape agrees reasonably well with the average shape computed from the recorded data for frequencies up to about 30 Hz. A possible site resonance near 25-30 Hz shows in the average spectral shape which then decreases rather monotonically with increasing frequency. This high frequency behavior beyond 50 Hz may be related to the damping in the stiff soil. Apart from the possible resonance effects, the model performs acceptably well in predicting average response spectral shapes for these small magnitude earthquakes.

Magnitude Scaling of WNA and ENA Spectral Shapes

50. Figure 22 shows the predicted magnitude scaling using WNA parameters (Table 1) with a kappa of 0.02 sec. As expected, the shapes saturate and are magnitude independent for frequencies higher than approximately 10 Hz. At lower frequencies, magnitude saturation is predicted in that at a given period, the change in the spectral level between magnitudes appears to be period dependent.

51. Interestingly, the value of maximum spectral amplification (near 2.5) is dependent upon magnitude. The period of maximum spectral amplification appears to increase with magnitude going from near 23 Hz for $M_w \approx 2.5$ to 11 Hz for $M_w \approx 5.5$. The value of maximum spectral amplification also appear to be magnitude dependent but only weakly so. Obser-

vations at one site, over a wide magnitude range, would be required to substantiate these model predictions. They are intriguing and are not predicted when using the f_{max} filter operator (Silva and Green, 1988).

52. Figure 23 shows the analogous scaling predictions using the ENA parameters listed in Table 1. As a consequence of the low kappa (0.006 sec), the typical pattern displayed by the WNA shapes has been shifted to higher frequencies. The maximum spectral amplification, approximately 2.3, is nearly the same as that of the WNA shapes but occurs at a higher frequency for corresponding magnitudes.

53. The offsets shown in the response spectral shape curves are due to changes in the estimated number of zero crossings in the oscillator response. The number of zero crossings (or extrema) is proportional to the ratio between the peak value and the RMS of the oscillator response (Boore, 1983).

Distance Scaling of WNA and ENA Spectral Shapes

54. The results for predicted WNA distance scaling of response spectral shapes for a M_W = 3.5 event are shown in Figure 24. The shapes are nearly identical from 5 to 25 km. This weak dependence upon distance was noted by Nuttli (1981) and is a consequence of the frequency dependence of Q(f) being roughly proportional to frequency above 1 Hz (Aki, 1985).

55. Figure 25 shows the distance scaling predicted for an M_W = 3.5 event using ENA parameters (Table 1). As with the WNA distance scaling, there is little effect of distance upon the spectral shapes. Since the ENA Q(f) model (Table 1) results in less long-period attenuation than that of the WNA model, the distance scaling is even less pronounced.

PART VI: EFFECTS OF DEPTH UPON RESPONSE SPECTRA AND FOURIER SPECTRA

Introduction and Theory

56. In general, earthquake-induced ground motions vary spatially, as well as with time. The spatial variation occurs both horizontally and vertically. This section will describe the effects of depth on Fourier amplitude and response spectra.

57. If we confine our attention to one-dimensional vertically propagating, linear waves, the variation of ground motion with depth is predictable (Haskell, 1960). Generally, one-dimensional, linear wave propagation models predict a decrease in ground motion with depth and the presence, at different depths and at specific frequencies, of nodes or nulls in the Fourier amplitude spectra.

58. The decrease in motion with depth is caused by a combination of the free surface effect and, normally, an increasing velocity with depth. If material damping is neglected, the increase in wave velocity with depth results in a decrease in the amplitude of the motion since the flow of energy per unit time and per unit area (energy flux) $\rho v_s \dot{u}^2$ (ρ = density, v_s = wave velocity, $\dot{u}$ = particle velocity) is conserved. Thus if v_s increases, $\dot{u}$ will decrease.

59. In considering the free surface effect, we treat the motion at depth and that at the surface as the sum of upgoing and downgoing (reflected) wavefields. At the surface, the stress-free condition requires that all frequency components of vertically upgoing and downgoing fields be exactly in phase, so that the surface motion is double that of either field. Beyond some depth (generally beyond 1/4 wavelength) the fields begin to separate, each with one-half the surface motion.

60. Interference of the upgoing and downgoing fields results in depth-dependent spectral nodes or minima at certain frequencies. These nodes are represented by a sinusoidal modulation of the Fourier spectrum of the surface motion. For a normally propagating shear wave in a half-space, the Fourier spectrum of the surface motion is multiplied by a cosine term, cos kz, where k is the wavenumber ($k = \omega/v_s = 2\pi/\lambda$, ω is the natural circular frequency and λ is the wavelength) and z is the depth. This term zeroes the Fourier spectrum every $(n/2 + 1/4)\lambda$ (n an integer) and results in depth-dependent spectral nodes. The implication for ground response analysis is that a broad-band spectrum cannot exist at arbitrary depths. Material damping (resulting in complex k) and layering complicate this simplified picture, but the basic principles still apply.

Observed Data From A Vertical Array

61. To illustrate the presence of the depth dependent nodes as well as the similarities and differences in response spectra and Fourier amplitude spectra regarding site response effects, data recorded at the Richmond Field Station (University of California, Berkeley) vertical array from the Briones Hills event ($M_L = 4.3$) are examined (Johnson and Silva, 1981).

62. The Richmond Field Station site is characterized by 35 m of Quaternary alluvium overlying bedrock of the Franciscan Formation of Jurassic - Cretaceous age. The alluvium consists of a combination of clay, silt, sand, and gravel with the water table generally standing only 2 m below the surface. Three component accelerometer packages are located at the surface, at 15 m depth, and in the bedrock at 40 m depth. The earthquake records used were from the 1977 Briones Hills, California main shock ($M_L = 4.3$). The peak acceleration recorded during the Briones Hills main shock was approximately 1% g. Analysis of the Fourier spectral density for these records and for windows preceding the earthquakes indicate a bandwidth with acceptable signal-to-noise ratio from about 3 seconds to 20 Hz.

63. Figures 26, 27, and 28 show the surface, mid-hole (15 m), and bottom (40 m) absolute acceleration response spectra and Fourier amplitude spectra. To average azimuthal effects, since the raypaths are near normal, we use the geometrical-mean of the spectra of both components rather than individual components.

64. The first three resonant frequencies, assuming a single layer overlying bedrock with an average surface to bedrock travel time of 0.142 seconds, are at 1.8, 5.4, and 9.0 Hz. These are indicated by arrows in Figure 26. The predicted maxima are reasonably well developed at nearly the predicted frequencies for both the response and Fourier amplitude spectra, with the exception of the fundamental response. It is predicted at 1.8 Hz, but is not well developed in the response spectra. For both spectra the third harmonic, predicted to occur at 9.0 Hz, is actually closer to 10 Hz, with minima occurring near 9 Hz. This may be due to interference from near-surface scattered waves, since the bottom (40m) Fourier amplitude spectra (Figure 28) shows well developed spectral nodes. The location of these nodes corresponds to the location of the maxima in the surface spectra and are again indicated with arrows. The fundamental depth node, expected at 1.8 Hz, is not apparent in the response spectra. This is analogous to the suppressed fundamental site response peak in the surface response spectra.

65. Figure 27 shows the response and Fourier amplitude spectra for the mid-hole data. Depth nodes are expected at 3.3, 9.7, and 16.7 Hz based upon a surface to mid-hole travel time of 0.076 sec. Again the depth nodes are well developed in the Fourier amplitude spectra and less so in the response spectra.

66. These results at the Richmond Field Station indicate that both response spectra and Fourier amplitude spectra are sensitive to depth effects in predictable ways. They also suggest that Fourier amplitude

spectra may provide overall better resolution of these effects than response spectra especially at higher frequencies where response spectra tend to display decreased resolution.

Model Predictions of Depth Effects

67. Synthetic Fourier amplitude and response spectra for a homogeneous rock site have been produced with the WES-RASCAL methodology to illustrate the model predictions of the effects of depth upon strong ground motion. Ground motion at depth within a half-space are analyzed. Motion is calculated at four locations: the surface of the half-space and at depths of 50, 100 and 150 m within the half-space.

68. The analysis consists of comparing Fourier amplitude and response spectral ratios between the surface and the three site depths. The half-space has an elastic shear-wave velocity of 3500 m/sec with a density of 2.5 gm/cm^3 and a constant damping ratio of 0.05% (Q = 1000).

69. The input motion is specified by a Brune spectrum utilizing ENA parameters (Table 1). Calculations are performed for moment magnitudes 3.0, 4.0, and 5.0 at a hypocentral range of 5 km. Fourier spectra at depth within the half-space are calculated by assuming vertically propagating plane shear-waves (Silva and Lee, 1987).

70. Results of the RVT calculations for the depths within the half-space are shown in the Figures 29 through 40. Figures 29 through 31 show the response spectral ratios for absolute acceleration at 5% damping between the surface and 50, 100, and 150 m for moment magnitudes 3.0, 4.0, and 5.0. Figure 32 shows the Fourier spectral ratios for the same parameters. Figures 33 through 38 show the individual Fourier amplitude spectra and response spectral velocity for M_w = 3.0, 4.0, and 5.0.

71. Comparison of Figures 29 through 38 reveal some interesting features. Both the response and Fourier spectral ratios display depth-dependent spectral nodes, however, the response spectral ratios have amplitudes which show some magnitude dependence. This suggests that a degree of caution is advisable when inferring the degree of motion reduction with depth from small magnitude data for application at larger magnitudes. Additionally, the spectral nodes in the response spectral ratios damp out beyond the second overtone for ENA ground motion parameters while those shown in the Fourier spectral ratios are much more predominant and are attenuated only slightly through the damping in the rock half-space.

72. The mechanism responsible for the magnitude dependence of the response spectral ratios may be related to an interaction of the earthquake source corner frequency and the depth node. The fundamental depth node is at approximately 16 Hz, 8 Hz and 4 Hz for depths of 50, 100 and 150 m, respectively. The corner frequencies for M_W 3.0, 4.0, and 5.0 are 10, 3, and 1 Hz respectively. We see from Figures 29 through 31 that the response spectral ratio is generally largest for magnitudes associated with corner frequencies farthest from the fundamental frequency of the depth node. The differences in amplitudes between the response spectral ratios and Fourier spectral ratios are due to the smoothing effect of damping in the oscillator response.

73. Fourier amplitude spectra (g-sec) and pseudo-relative velocity response spectra (cm/sec) computed at the rock outcrop and at depths of 50, 100, and 150 m for M_W = 5.0 are shown in Figures 33 and 34. Analogous plots for M_W 4.0 and 3.0 are shown in Figures 35 through 38. The figures all show the depth-dependent spectral nodes with the outcrop motion representing the upper bound at all periods.

74. Figures 39 and 40 show the variation with depth of peak ground acceleration and particle velocity at a hypocentral distance of 5 km for M_W of 3.0, 4.0, and 5.0. In Figure 39, the peak acceleration decreases

rapidly in the first 20 to 40 m and remains fairly constant for depths below 40 m. As expected, the largest peak accelerations occur at the free-surface. In Figure 40, the peak ground particle velocity, decreases more slowly with depth because it is associated with lower frequencies than peak acceleration. Again, the largest particle velocity occurs at the free-surface.

PART VII: SUMMARY AND CONCLUSIONS

75. This report demonstrates that response spectral shapes and acceleration time histories computed for small magnitude earthquakes using the BLWN ground motion model combined with random vibration theory agree well with spectral shapes computed from observed WNA and ENA recordings on rock and stiff soil and to recorded acceleration time histories. Comparisons were made for moment magnitudes of approximately 2.5 to 5.3 at distances predominately within 25 km of the source. A site dependent kappa of 0.02 - 0.03 sec appeared reasonable for WNA motions recorded on hard rock (crystalline) and soft rock (sedimentary) sites, respectively. For data recorded at the Anza array, within the Southern California batholith, a kappa of 0.009 sec provided the closest match to response spectral shapes computed from the observed data. A kappa of 0.006 sec was required to match the data recorded at ENA sites on rock while a kappa of 0.0094 sec provided the best fit to shapes computed from data recorded on stiff soil.

76. Ground motions recorded in ENA at rock or very stiff soil sites contain significantly more high frequency energy than corresponding ground motions recorded at typical rock sites in WNA. This results in a shift in spectral shape to higher frequencies. However, WNA motions can have response spectral content similar to that typical of ENA rock motions for sites located on very hard crystalline rock.

77. Five percent response spectral shapes for small magnitude earthquakes are predicted to have a magnitude dependent period of maximum amplification which increases with magnitude. This dependence is stronger for typical WNA motions than for ENA motions. Response spectral shapes at these small magnitudes have a strong dependence upon magnitude and a very weak dependence upon distance in the hypocentral range of 5 to 25 km.

78. For ENA small magnitudes earthquakes, peak acceleration is predicted to decrease rapidly with depth for the first 20 to 30 m within a homogenous rock mass. At these depths, the peak acceleration is at approximately 70% of its value at the free-surface and remains nearly constant down to 200 m. Peak particle velocity decreases less rapidly with depth than does peak acceleration due to its lower frequency content. Spectral nodes in Fourier and response spectra are shown to occur at depth with data from a vertical array. The nodes are predicted analytically by the ground motion model and are a consequence of interference between upgoing and downgoing waves.

REFERENCES

Aki, K., 1985, Attenuation and site effects at high frequency, in Strong ground motion simulation and earthquake engineering applications, Earthquake Engineering Research Institute, No. 85-02, p. 23-1, November.

Anderson, J.G., and Hough, S.E., 1984, A model for the shape of the Fourier amplitude spectrum of acceleration at high frequencies: Bulletin of the Seismological Society of America, Vol. 74, No. 5, pp. 1969-1993, October.

Algermissen, S.T., and Campbell, K.W., 1985, Near-source estimation of strong ground motion for the eastern United States: in Second Quarter Progress Report - FY 85 to Nuclear Regulatory Commission.

Atkinson, G.M., 1984, Attenuation of strong ground motion in Canada: Bulletin of the Seismological Society of America, Vol. 74, No. 6, pp. 2629-2953, December.

Berger, J., Baker, L.M., Brune, J.N., Fletcher, J.B., Hanks, T.C., and Vernon, F.L., III, 1984, The Anza array: A high-dynamic-range, broadboard, digitally radio telemetered seismic array: Bulletin of the Seismological Society of America, Vol. 74, No. 4, pp 1469-1481, August.

Boore, D. M., 1983, Stochastic simulation of high-frequency ground motions based on seismological models of the radiated spectra: Bulletin of the Seismological Society of America, Vol. 73, No. 6, Part A, pp. 1865-1984, December.

Boore, D. M., 1986a, Short-period P- and S-wave radiation from large earthquakes: Implications for spectral scaling relations: Bulletin of the Seismological Society of America, Vol. 76, No. 1, pp. 43-64, February.

Boore, D.M., and Atkinson, G.M., 1987, Prediction of ground motion and spectral response parameters at hard-rock sites in eastern North America: Bulletin of the Seismological Society of America, Vol. 77, No. 2, pp. 440-467, April.

Boore, D.M., and Joyner, W.B., 1984, A note on the use of random vibration theory to predict peak amplitudes of transient signals: Bulletin of the Seismological Society of America, Vol. 74, No. 5, pp. 2035-2039, October.

Borcherdt, R.D., 1986, Preliminary report on aftershock sequence for earthquake of January 31, 1986 near Painesville, Ohio: U.S. Geological Survey Open-File Report 86-181.

Borcherdt, R.D., Fletcher, J.B., Jensen, E.G., Maxwell, G.L., Van Schaack, J.R., Warrick, R.E., Cranswick, E., Johnston, M.J.S., and McClearn, R., 1985, A General Earthquake Observation System (GEOS): Bulletin of the Seismological Society of America, Vol. 75, No. 6, pp. 1783-1823, December.

Borcherdt, R.D., and Glassmoyer, G., 1987, On the aftershock sequence for the earthquake of January 31, 1986 in northeastern Ohio: Effects of bandwidth and local geology on observed high-frequency ground motion: Workshop on Earthquake Ground Motion Estimation in Eastern North America, Electric Power Research Institute, March 31 - April 2.

Brune, J.N., 1970, Tectonic stress and the spectra of seismic shear waves from earthquakes: Journal of Geophysical Research, Vol. 75, pp. 4997-5009, September.

Brune, J.N., 1971, Correction: Journal of Geophysical Research, Vol. 76, p. 5002, July.

Burger, R.W., Somerville, P.G., Barker, J.S., Herrmann, R.B., and Helmberger, D.V., 1987, The effect of crustal structure on strong ground motion attenuation relations in eastern North America: Bulletin of the Seismological Society of America, Vol. 77, No. 2, pp. 420-439, April.

Campbell, K.W., 1985, Near-source estimation of strong ground motion for the eastern United States: Second quarter progress report - FY 1985 to Nuclear Regulatory Commission, 14 p.

Chang, F.K., 1983, Analysis of strong-motion data from the New Hampshire earthquake of 18 January 1982, Nuclear Regulatory Commission, NUREG/CR-3327.

Cranswick, E., Wetmiller, R., and Boatwright, J., 1985, High-frequency observations and source parameters of microearthquakes recorded at hard-rock sites: Bulletin of the Seismological Society of America, Vol. 75, No. 6, pp. 1535-1567, December.

Haar, L.C., Fletcher, J.B., and Mueller, C.S., 1984, The 1982 Enola, Arkansas swarm and scaling of ground motion in the eastern United States: Bulletin of the Seismological Society of America, Vol. 74, No. 6, pp. 2463-2482, December.

Hanks, T.C., 1979, b values and $\omega^{-\gamma}$ seismic source models: Implications for tectonic stress variations along active crustal fault zones and the estimation of high-frequency strong ground motion, Journal of Geophysical Research, Vol. 84, No. B5, pp. 2235-2242, May.

Hanks, T.C., 1982, fmax: Bulletin of the Seismological Society of America, Vol. 72, No. 6, pp. 1867-1879, December.

Hanks, T.C., and Kanamori, H., 1979, A moment magnitude scale: Journal of Geophysical Research, Vol. 84, pp. 2348-2350, May.

Hanks, T.C., and McGuire, R.K., 1981, The character of high-frequency strong ground motion: Bulletin of the Seismological Society of America, Vol. 71, No. 6, pp. 2071-2095, December.

Haskell, N.A., 1960, Crustal reflections of plane SH waves: Journal of Geophysical Research, Vol. 65, pp. 4147-4150.

Hough, S.E., and Anderson, J.G., 1988, High-frequency spectra observed at Anza, California: Implications for Q structure: Bulletin of the Seismological Society of America, Vol. 78, No. 2, pp. 692-707, April.

Johnson, L.R. and Silva, W. (1981). The effects of unconsolidated sediments upon the ground motion during local earthquakes: Bulletin of the Seismological Society of America, Vol. 71, No. 1, pp. 127-142, February.

Joyner, W.B. and T.E. Fumal, 1985, Predictive mapping of earthquake ground motion: in Evaluating Earthquake Hazards in the Los Angeles Region - An Earth-Science Perspective, U.S. Geological Survey Professional Paper 1360, pp. 203-220.

McGuire, R.K., and Hanks, T.C., 1980, RMS accelerations and spectral amplitudes of strong ground motion during the San Fernando, California, earthquake: Bulletin of the Seismological Society of America, Vol. 70, No. 5, pp. 1907-1920, October.

McGuire, R.K., Becker, A.M., and Donovan, N.C., 1984, Spectral estimates of seismic shear waves: Bulletin of the Seismological Society of America, Vol. 74, No. 4, pp. 1427-1440, August.

Nuttli, O.W., 1981, Similarities and differences between western and eastern United States earthquakes, and their consequences for earthquake engineering: in Beavers, J.E., ed., Proceedings, Conference on Earthquakes and Earthquake Engineering - Eastern United States, Knoxville, Tennessee, September 14-16, Ann Arbor Science Publishers.

Nuttli, O.W., Rodriquez, R., and Herrmann, R.B., 1986, Strong Ground Motion Studies for South Carolina Earthquakes, NUREG/CR-3755.

Papageorgiou, A.S., and Aki, K., 1983, A specific barrier model for the quantitative description of inhomogeneous faulting and the prediction of strong ground motion, Part II, Applications of the model: Bulletin of the Seismological Society of America, Vol. 73, No. 4, pp. 953-978, August.

Silva, W.J., and Green, R.K., 1988, Magnitude and distance scaling of response spectral shapes for rock sites with applications to North American tectonic environments: paper submitted for publication to Earthquake Spectra, Earthquake Engineering Research Institute.

Silva, W.J., and Lee, K., 1987, WES RASCAL code for synthesizing earthquake ground motions: State-of-the-Art for Assessing Earthquake Hazards in the United States, Report 24, U.S. Army Corps of Engineer Waterways Experiment Station, Vicksburg, Mississippi, Miscellaneous Paper S-73-1, 120p., May.

Toro, G.R., 1985, Stochastic model estimates of strong ground motion: in McGuire, R.K., ed., Seismic Hazard Methodology for Nuclear Facilities in the Eastern United States, Appendix B, Electric Power Research Institute, Project P101-29, April.

Toro, G.R., and McGuire, R.K., 1987, An investigation into earthquake ground motion characteristics in eastern North America: Bulletin of the Seismological Society of America, Vol. 77, No. 2, pp. 468-489, April.

Wesson, R.L., and Nicholson, C., 1986, Studies of the January 31, 1986 northeastern Ohio earthquake: Report to the U.S. Nuclear Regulatory Commission, U.S. Geological Survey Open-File Report 86-331, 131 p.

Wetmiller, R.J., Horner, R.B., Hasegawa, H.S., North, R.G., Lamontagne, M., Weichert, D.H. and, Evans, S.G., 1988, An analysis of the 1985 Nahanni earthquakes: Bulletin of the Seismological Society of America, Vol. 78, No. 2, pp. 590-616, April.

Wiechert, D.H., Wetmiller, R.J., Horner, R.B., Munro, P.S., and Mork, P.N., 1986, Strong motion records from the 23 December 1985, Ms 6.9 Nahanni, NWT, and some associated earthquakes: Geological Survey of Canada Open File Report 1330.

Table 1

EARTHQUAKE SOURCE AND WAVE PROPAGATION PARAMETERS

Parameters	Western North America (WNA)	Eastern North America (ENA)
ρ (g/cm^3)	2.7	2.5
β (km/sec)	3.2	3.5
Kappa (sec)	0.020	0.006
$Q(f)$*	$150(f)^{0.6}$	$500\ (f)^{0.65}$
$\Delta\sigma$ (bars)	50	100
M_o (dyne-cm)	$\log M_o = 1.5\ M_w + 16.1$	$\log M_o = 1.5\ M_w + 16.1$
Amplification Factors	See Table 2	1.0
Geometrical Attenuation	R^{-1}	R^{-1}
Source Duration	f_c^{-1}	f_c^{-1}
f_c	$\beta^3 \Delta\sigma / 8.44\ M_o$	$\beta^3 \Delta\sigma / 8.44\ M_o$

* WNA from Nuttli (1986); ENA from Toro (1985)

Table 2

NEAR SURFACE AMPLIFICATION FACTORS
(From Boore, 1986)

Log Frequency	$\log \left(\frac{\beta_o \rho_o}{\beta_R \rho_R}\right)^{\frac{1}{2}*}$
-1.0	0.01
-0.5	0.04
0.0	0.13
0.5	0.34
1.0	0.37

*ρ_o and ρ_R are assumed to be equal.

o,R refers to average crustal properties and near-receiver properties, respectively.

Table 3

EARTHQUAKES AND STATIONS USED FOR WNA M_w = 5.3 COMPARISON

Earthquake	Date	Magnitude (M_L)	Source Depth (km)	Epicentral Distance (km)	USGS Station	No.	Average Horizontal Peak Acceleration (g)
Lytle Creek	700912	5.4	8.0	45.2	Santa Anita	104	0.033
Coalinga (2)	830509	5.1	12.5	14.0	Baths	46T03	0.007
				3.0	Anticline (Palmer)	46T05	0.233
				6.0	Skunk	46T06	0.315
(4)	830709	5.3	9.5	12.0	Baths	46T03	0.059
(6)	830722	5.0	9.5	10.0	Baths	46T03	0.035
(7)	830725	5.1	9.5	10.0	Baths	46T03	0.185
(8)	830909	5.3	9.5	13.0	Baths	46T03	0.014

Table 4

EARTHQUAKES AND SITES USED FOR ENA M_w = 5.3 COMPARISON

Earthquake	Date	Magnitude (m_b)	Source Depth (km)	Epicentral Distance (km)	Station	Average Horizontal Peak Acceleration (g)
Nahanni	851223	5.4	6		Site #1	0.10
Nahanni	851225	5.7	6	18	Site #3	0.10

Table 5

EARTHQUAKES AND STATIONS USED FOR WNA M_W = 4.5 COMPARISON

Earthquake	Date	Magnitude (M_L)	Source Depth (km)	Epicentral Distance (km)	USGS Station No.		Average Horizontal Peak Acceleration (g)
Oroville (K)	750808	4.9	6.4	5.8	6	1551	0.177
(N)	750811	4.3	0.5	2.5	6	1551	0.344
(P)	750816	4.0	8.8	3.6	6	1551	0.098
				5.7	8	1495	0.054
(T)	750926	4.0	9.4	5.2	6	1551	0.079
				7.1	8	1495	0.053
				17.6	9	1552	0.041
(U)	750927	4.6	8.4	10.2	8	1495	0.113
				20.8	9	1552	0.054

Table 6

EARTHQUAKES AND STATIONS USED FOR ENA M_w = 4.5 COMPARISON

Earthquake	Date	Magnitude	Source Depth (km)	Epicentral Distance (km)	Station	Average Horizontal Peak Acceleration (g)
New Brunswick	820331	4.8 (M_N)	5**	6	Holmes Lake	0.26
		4.01 (M_w)*		4	Mitchell Rd	0.20
				6	Loggie Lodge	0.44
				3	Indian Brook	0.42
New Brunswick	820506	4.8 (M_N)	5**	7	Loggie Lodge	0.13
New Hampshire	820119	4.7 (M_L)	8**	8	Franklin Falls Dam Crest	0.18
		4.36 (M_w)*		8	Franklin Falls Dam Downstream	0.19
				8	Franklin Falls Dam Right Abutment	0.43
				60	Union Village Crest	0.03
				60	Union Village Dam Downstream	0.03
				60	Union Village Left Abutment	0.01
Nahanni	851109	4.7 (M_N)	18	6	Site #2	0.43

* = (After Boore and Atkinson, 1987)
** = (After Toro and McGuire, 1987)

Table 7

EARTHQUAKES AND STATIONS USED FOR WNA M_W = 2.5 COMPARISON

Earthquake*	Date	Magnitude (M_L)	Source Depth (km)	Epicentral Distance (km)	Station	Name	Average Horizontal Peak Acceleration (g)
Anza	821017	2.6	7.3	8.6	#1	PFO	0.0047
	821028	2.4	17.7	26.3	#1	PFO	0.00049
				0.4	#2	KNW	0.0018
	821116	2.7	8.8	17.4	#1	PFO	0.00052
				26.3	#2	KNW	0.00038

* Microearthquakes recorded at the Anza array in California.

Table 8

EARTHQUAKES AND STATIONS USED FOR ENA M_w = 2.5 COMPARISON

Earthquake	Date	Magnitude	Source Depth (km)	Epicentral Distance (km)	Station	Average Horizontal Peak Acceleration (g)
Painesville	860203	2.1 M_{coda}	6	10	Station #2	0.0029
			1.5		Station #3	0.0058
Painesville	860206	2.5 M_{coda}	6	10	Station #2	0.013
			1.5		Station #3	0.016

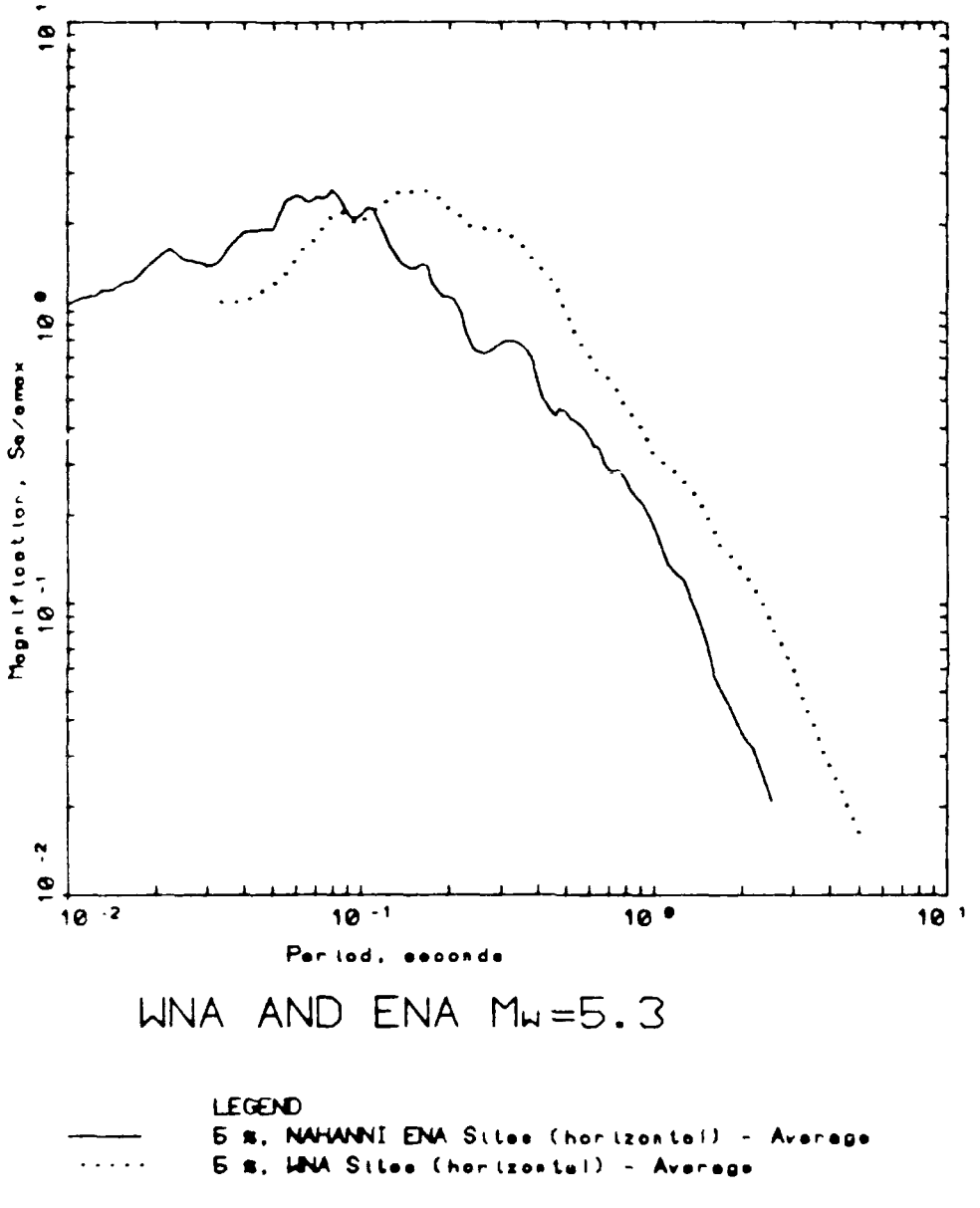

Figure 1 - Comparison of average 5% response spectral shapes (Sa/a_{max}) computed from strong motion data recorded at rock sites in ENA (solid line) and WNA (dotted line). WNA data are listed in Table 3 and ENA data are listed in Table 4.

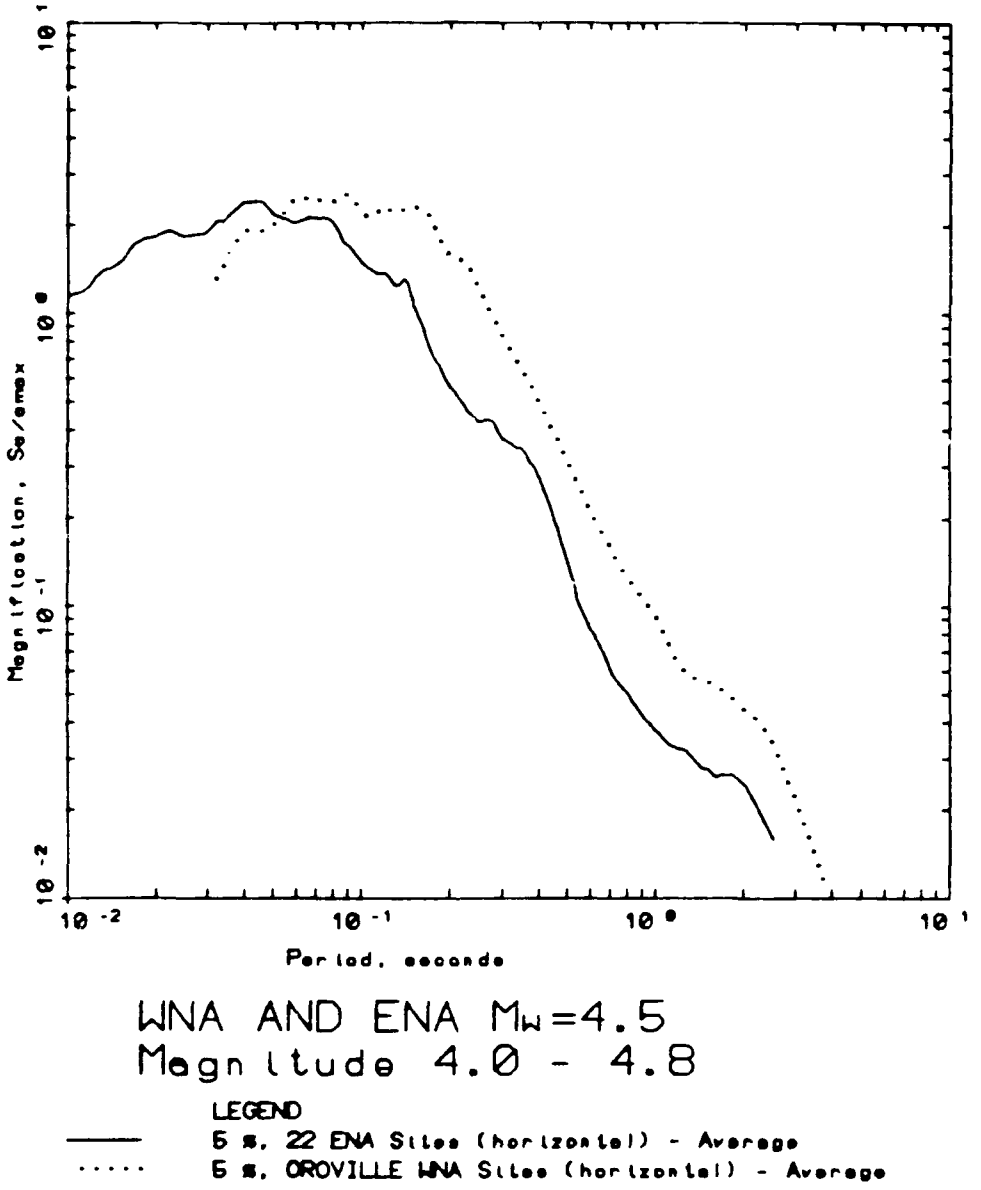

Figure 2 - Comparison of average 5% response spectral shapes (Sa/a_{max}) computed from strong motion data recorded at rock sites in ENA (solid line) and WNA (dotted line). The WNA average shape is from aftershocks of the Oroville earthquake listed in Table 5. The ENA average shape is from recordings listed in Table 6.

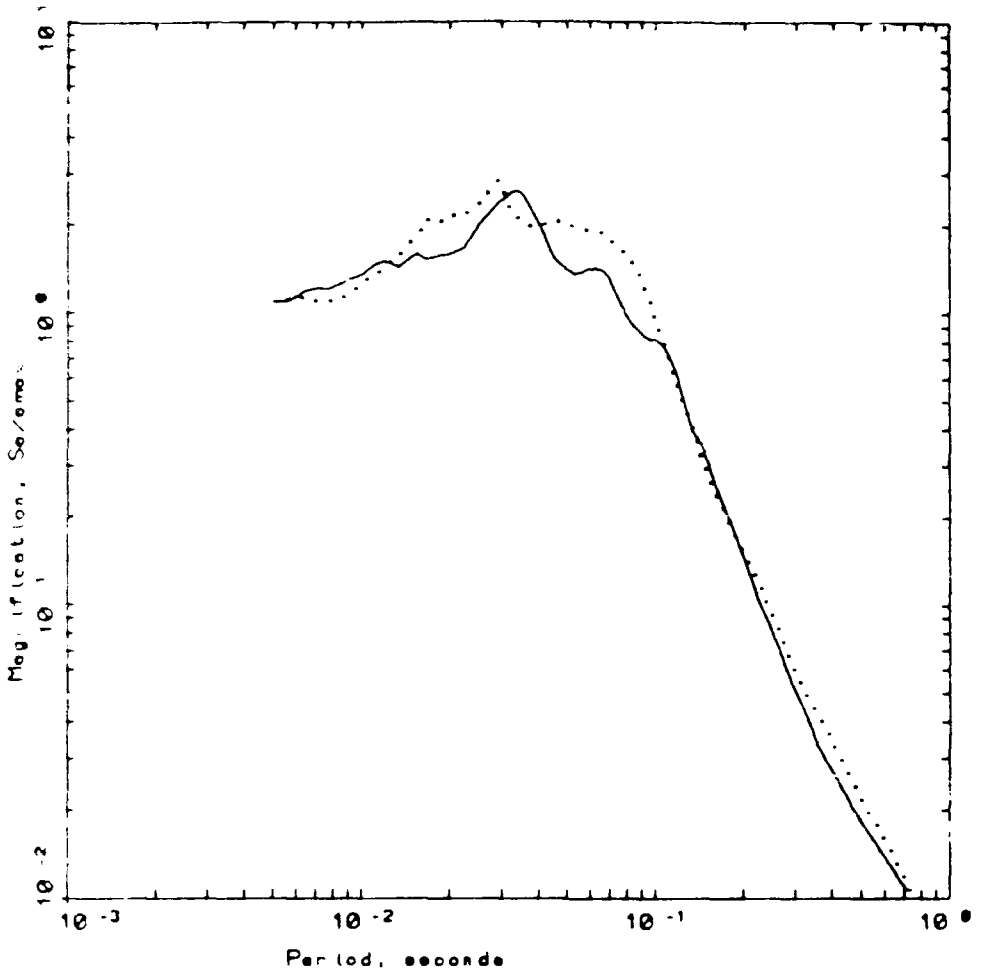

Figure 3 - Comparison of average 5% response spectral shapes (Sa/a_{max}) computed from strong motion data recorded at rock sites in ENA (solid line) and WNA (dotted line). The WNA average shape is from earthquakes recorded by the Anza array listed in Table 7. The ENA average shape is from recordings of aftershocks of the Painesville, Ohio earthquake listed in Table 8.

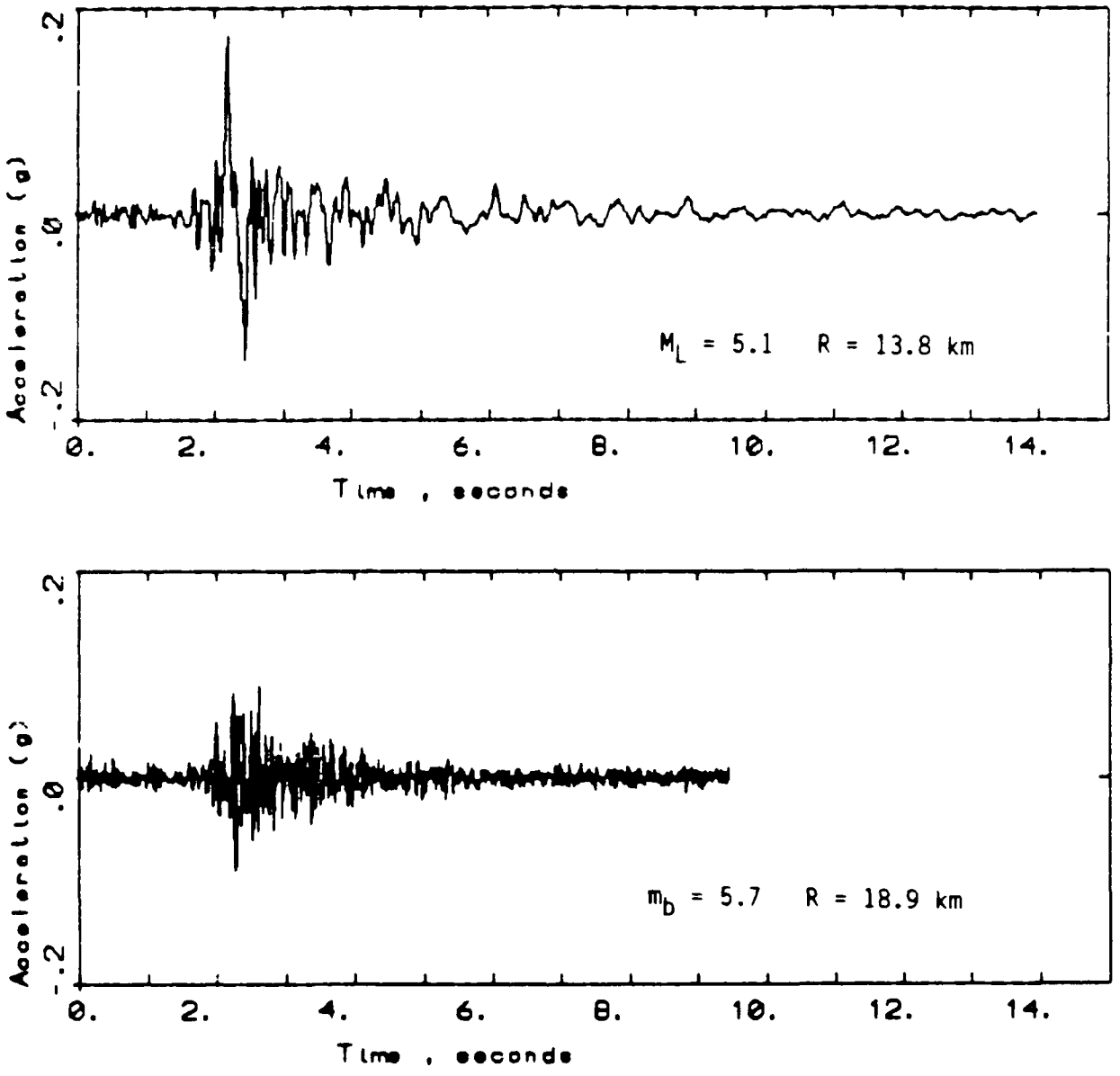

Figure 4 - Top trace: WNA accelerogram recorded at Sulphur Baths during the July 25, 1983 Coalinga aftershock (Table 3). Bottom trace: ENA accelerogram recorded at Site #3 during the December 25, 1985 Nahanni aftershock (Table 4).

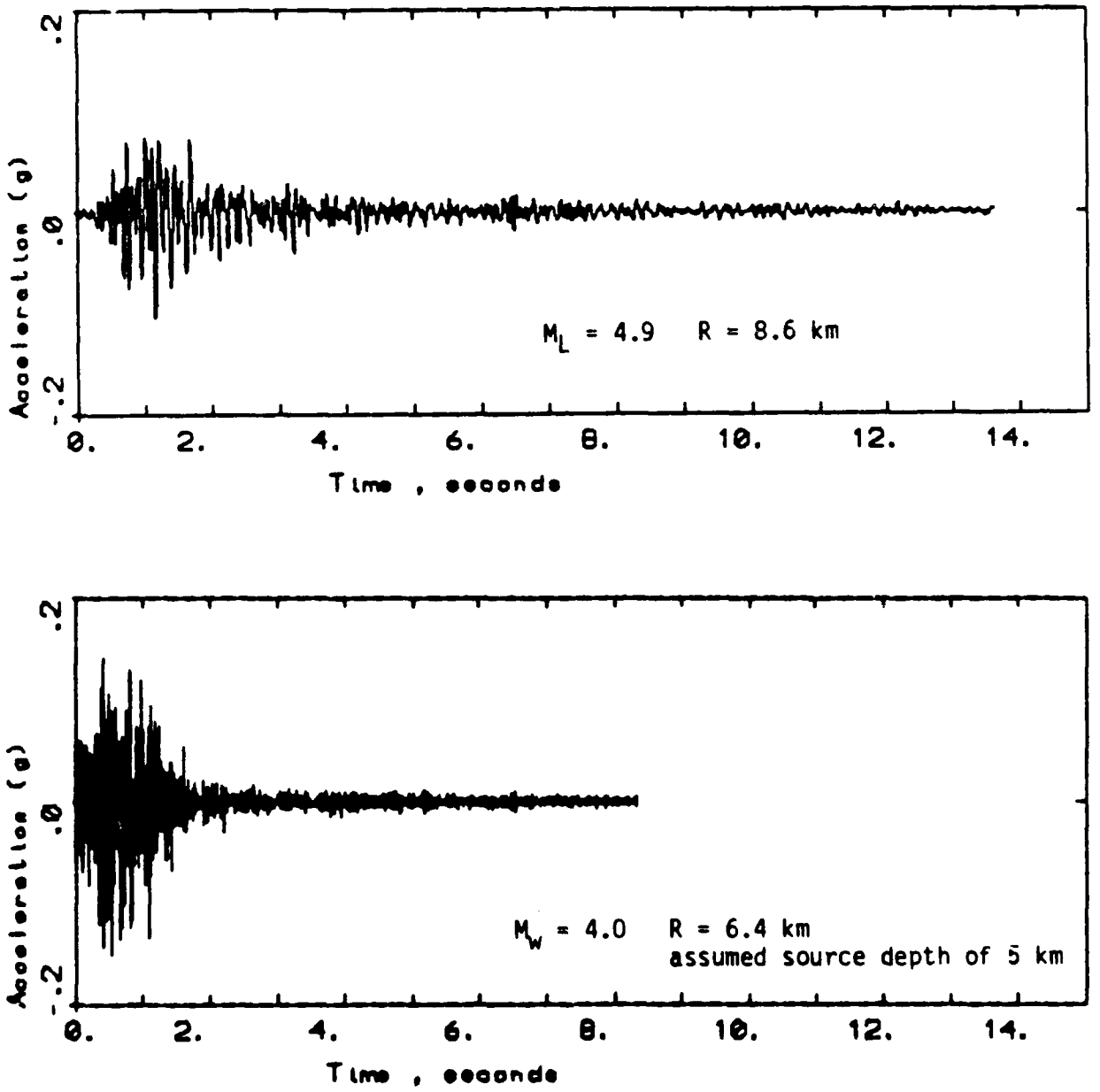

Figure 5 - Top trace: WNA accelerogram recorded at Station #6 during the August 8, 1975 Oroville aftershock (Table 5). Bottom trace: ENA accelerogram recorded at Mitchell Road during the March 31, 1982 New Brunswick aftershock (Table 6).

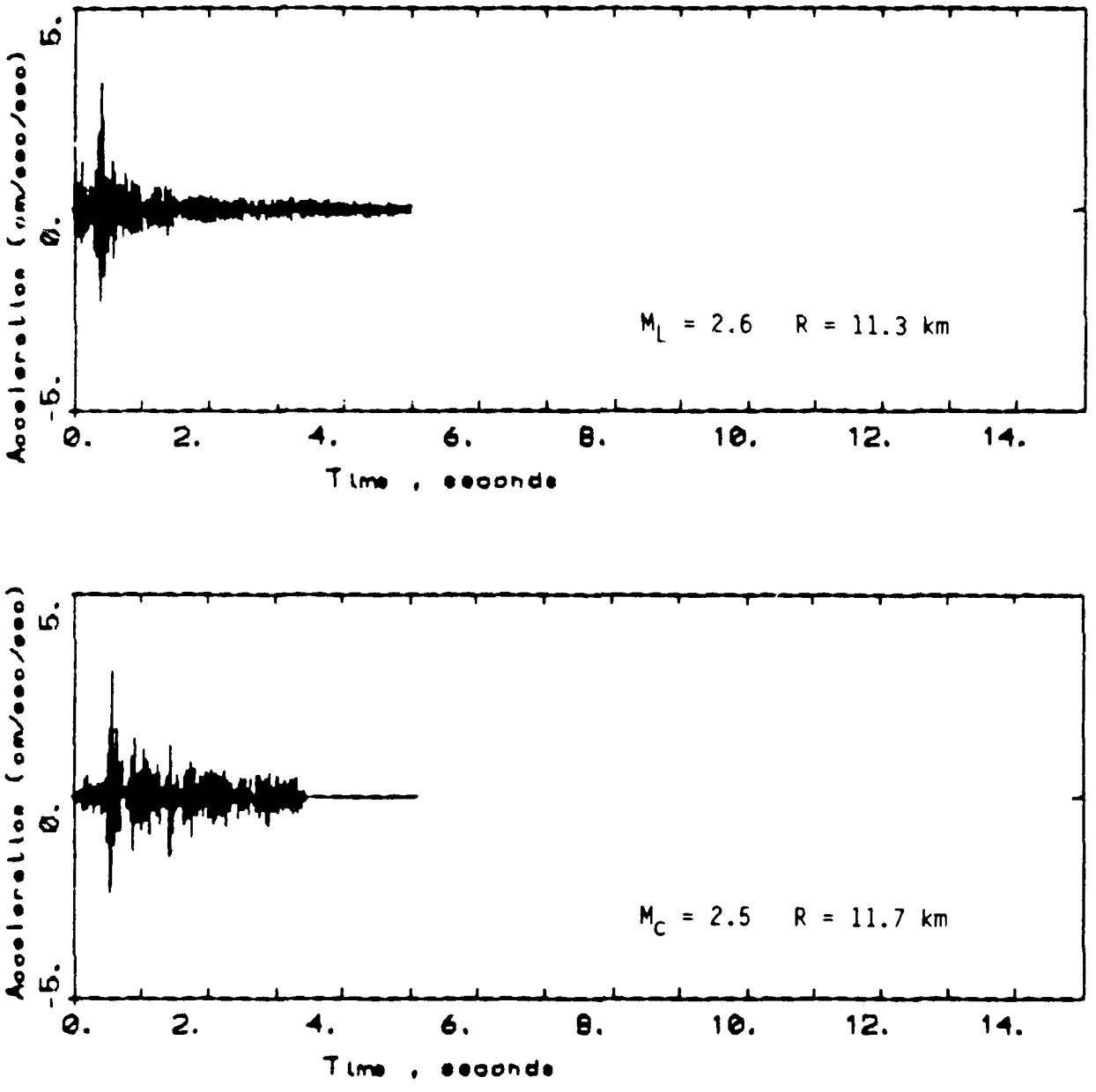

Figure 6 - Top trace: WNA accelerogram recorded at the Anza array (Station PFO) for the October 17, 1982 microearthquake (Table 7). Bottom trace: ENA accelerogram recorded at Station #2 during the February 6, 1986 Painesville aftershock (Table 8).

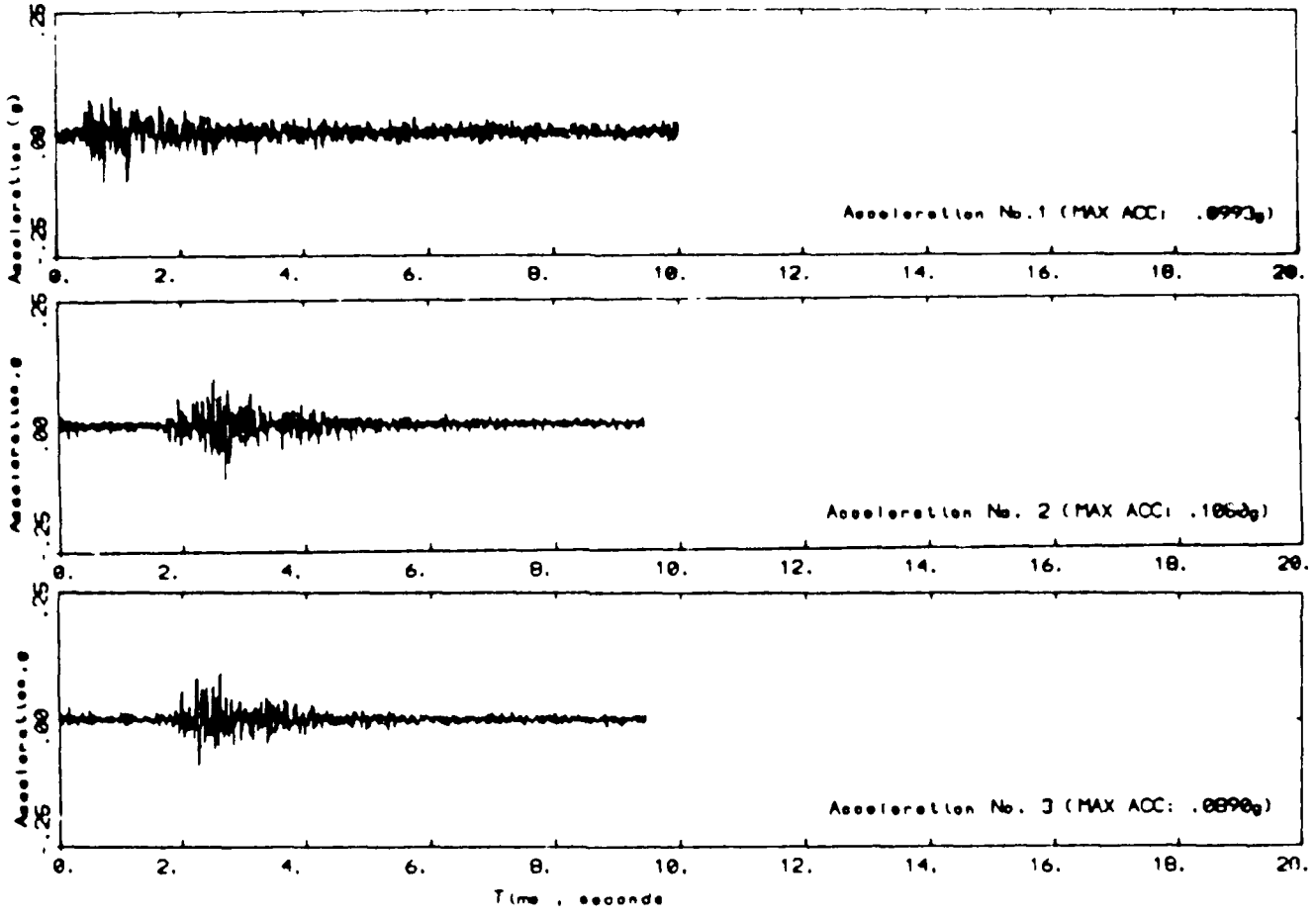

Figure 7 - Comparison of a synthetic accelerogram (Acceleration No. 1) generated as described in Part IV to two examples of recorded ground accelerations (Acceleration No. 2 and No. 3) at a distance of 25 km for M_w = 5.3 using ENA parameters (Table 1).

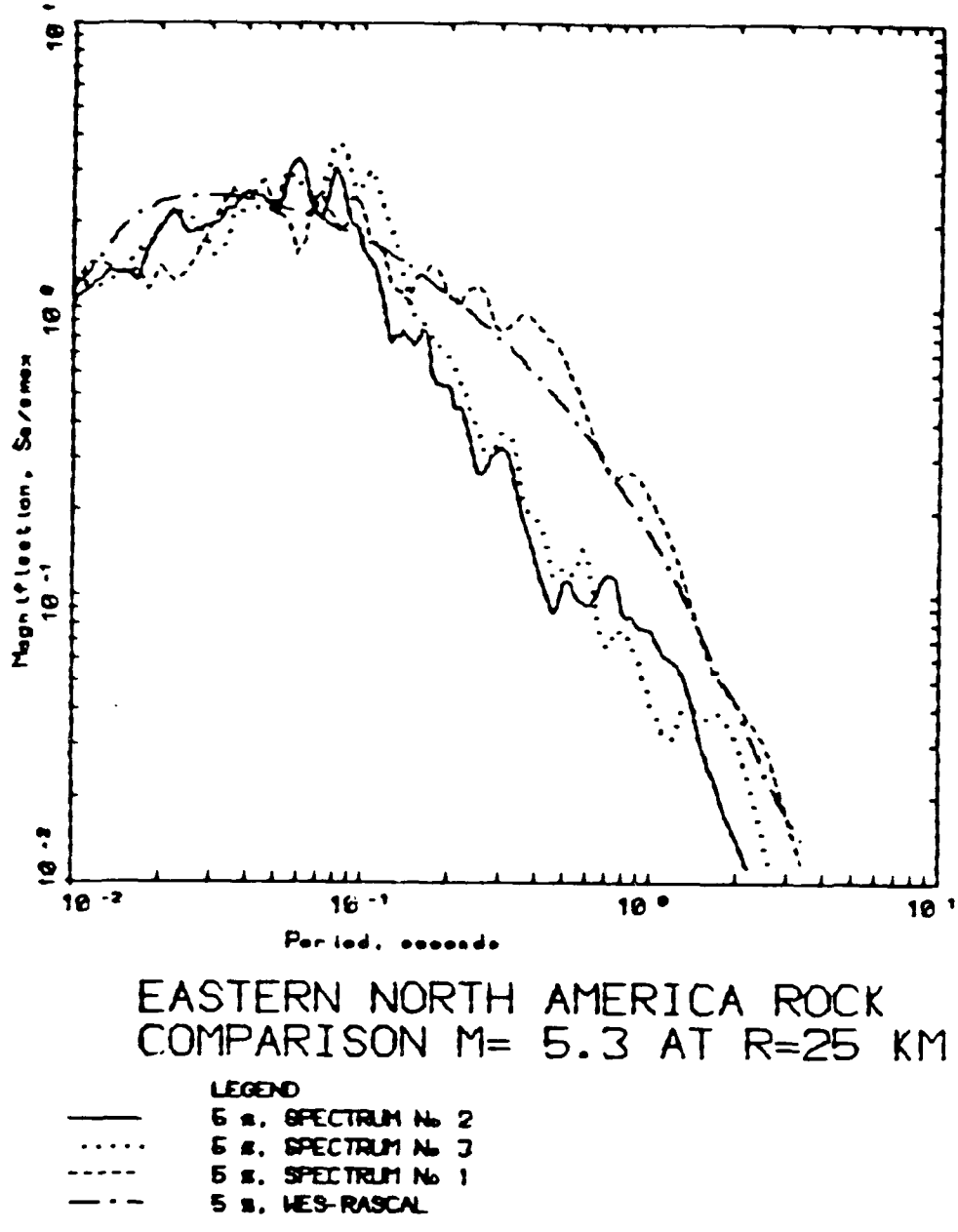

Figure 8 - Comparison of 5% response spectral shapes for the accelerograms in Figure 7. The WES-Rascal RVT estimate is the dashed - dot curves. The BLWN Fourier amplitude spectral estimate combined with the phase of an observed accelerogram is the dashed line (Spectrum 1). The 5% response spectral shapes of the recorded ground accelerations are the solid line (Spectrum 2) and the dotted line (Spectrum 3) for M_w = 5.3 at a distance of 25 km.

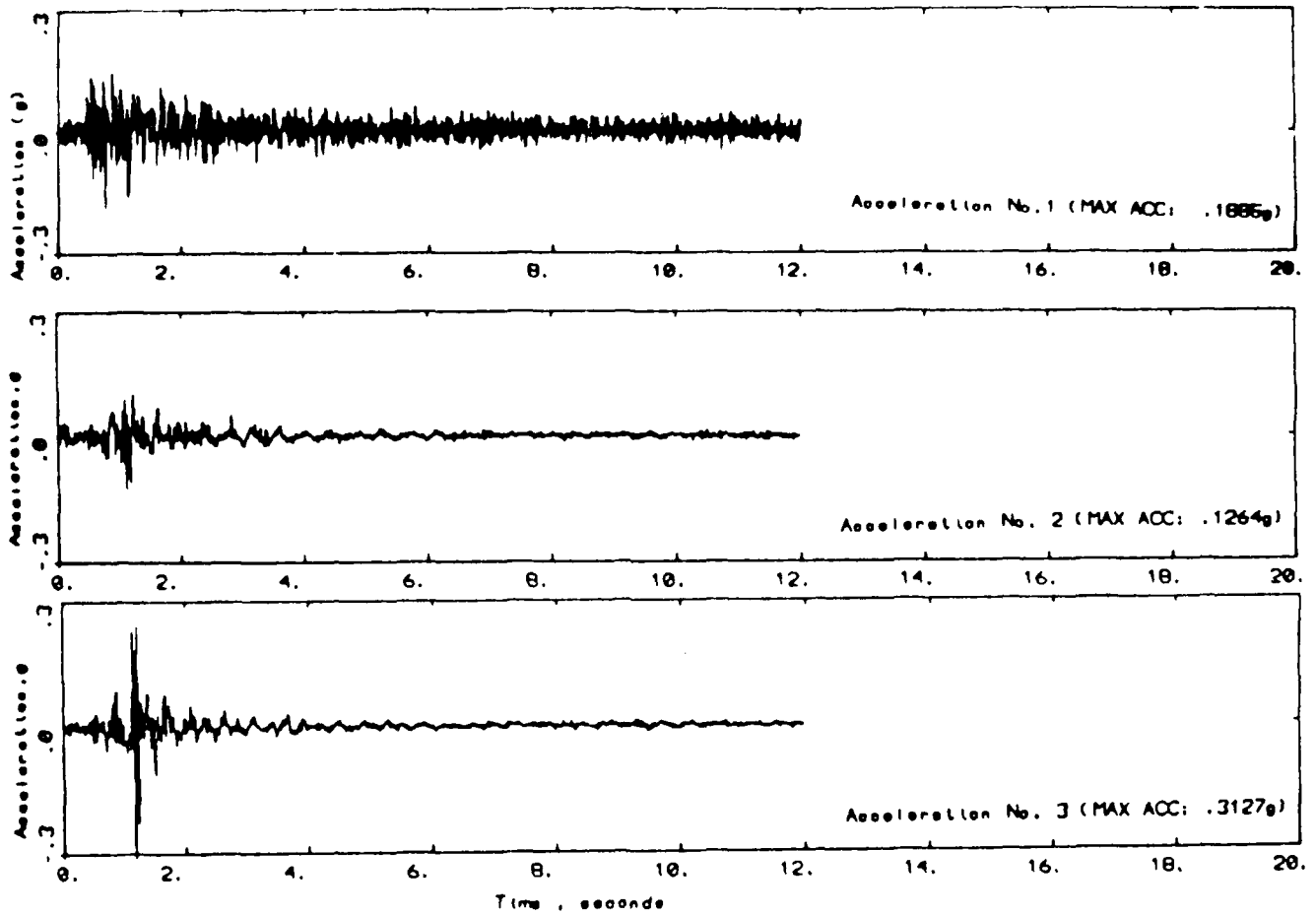

Figure 9 - Comparison of synthetic accelerogram (Acceleration No. 1) generated as described in Part IV to two examples of recorded ground accelerations (Acceleration No. 2 and No. 3) at a distance of 8 km for M_w = 4.5 using ENA parameters (Table 1).

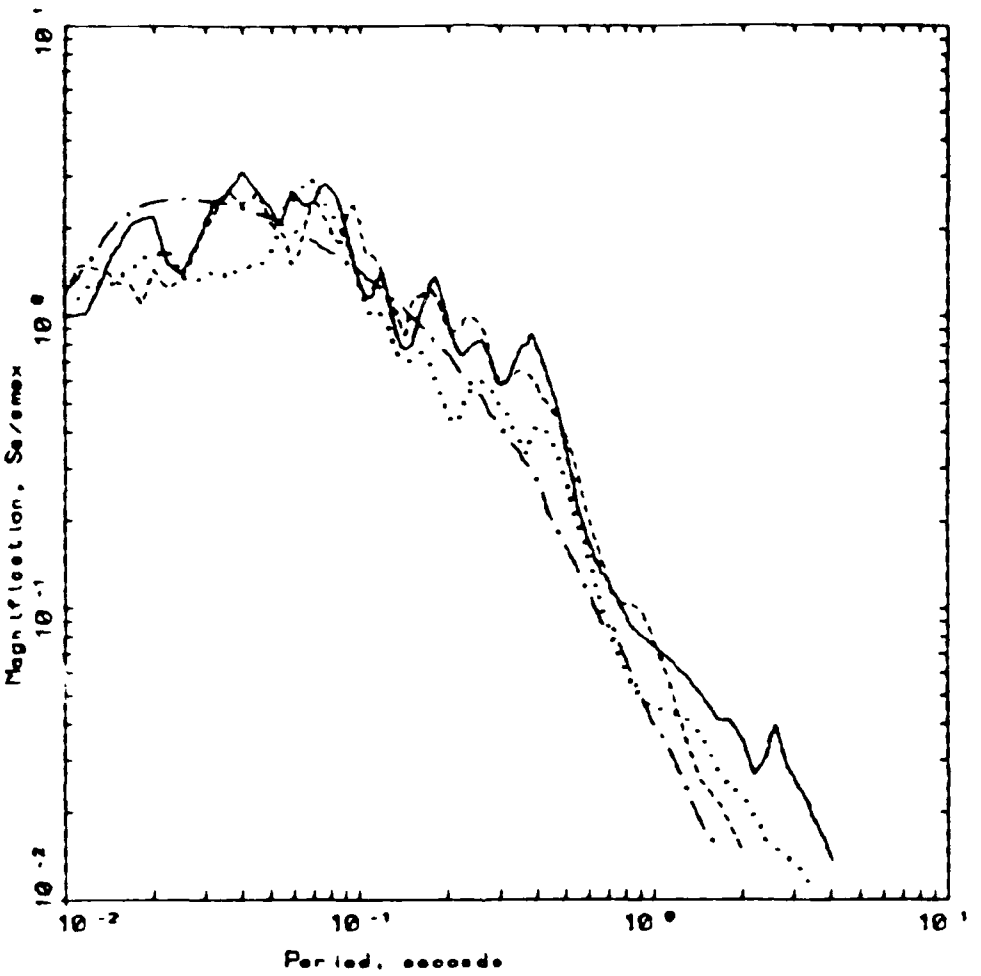

Figure 10 - Comparison of 5% response spectral shapes for the accelerograms in Figure 9. The WES-Rascal RVT estimate is the dashed - dot curve. The BLWN Fourier amplitude spectral estimate combined with the phase of an observed accelerogram is the dashed line (Spectrum 1). The 5% response spectral shapes of the recorded ground accelerations are the solid line (Spectrum 2) and the dotted line (Spectrum 3) for M_w = 4.5 at a distance of 8 km.

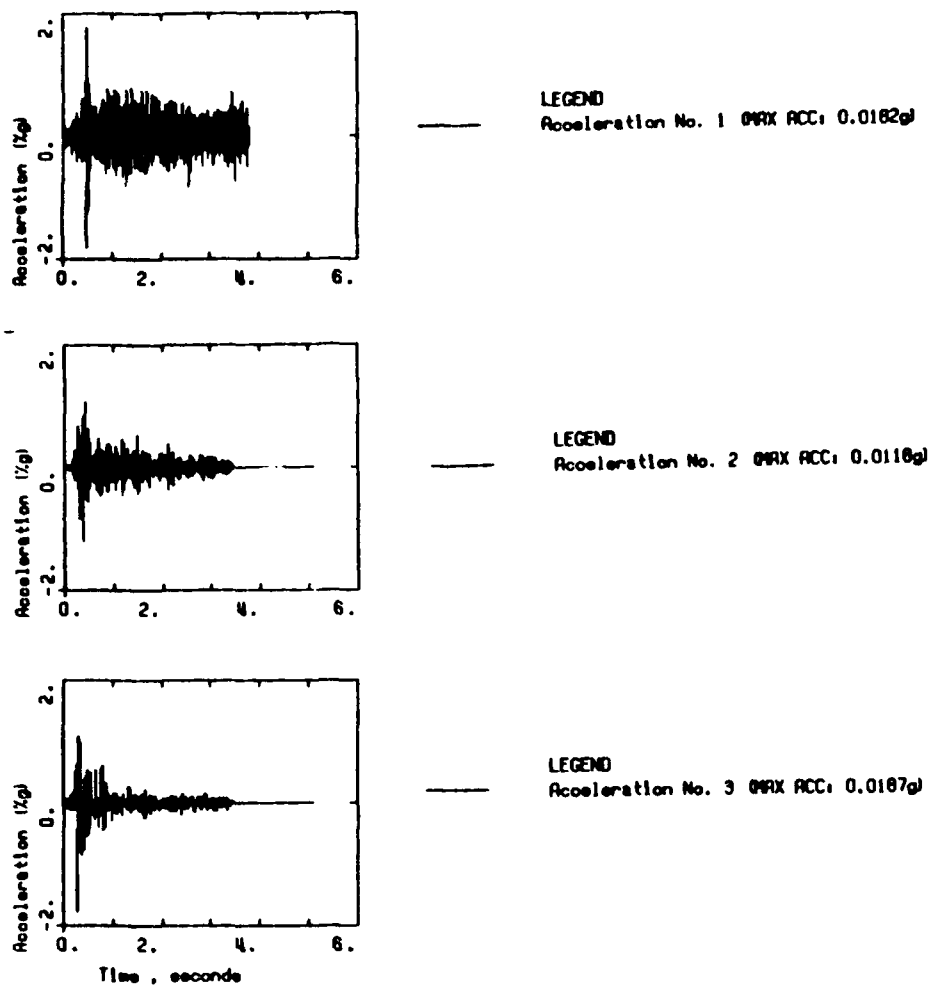

Figure 11 - Comparison of a synthetic accelerogram (Acceleration No. 1) generated as described in Part IV to two examples of recorded ground accelerations (Accelerations No. 2 and No. 3) at a distance of 10 km for M_w = 2.5 using ENA parameters (Table 1).

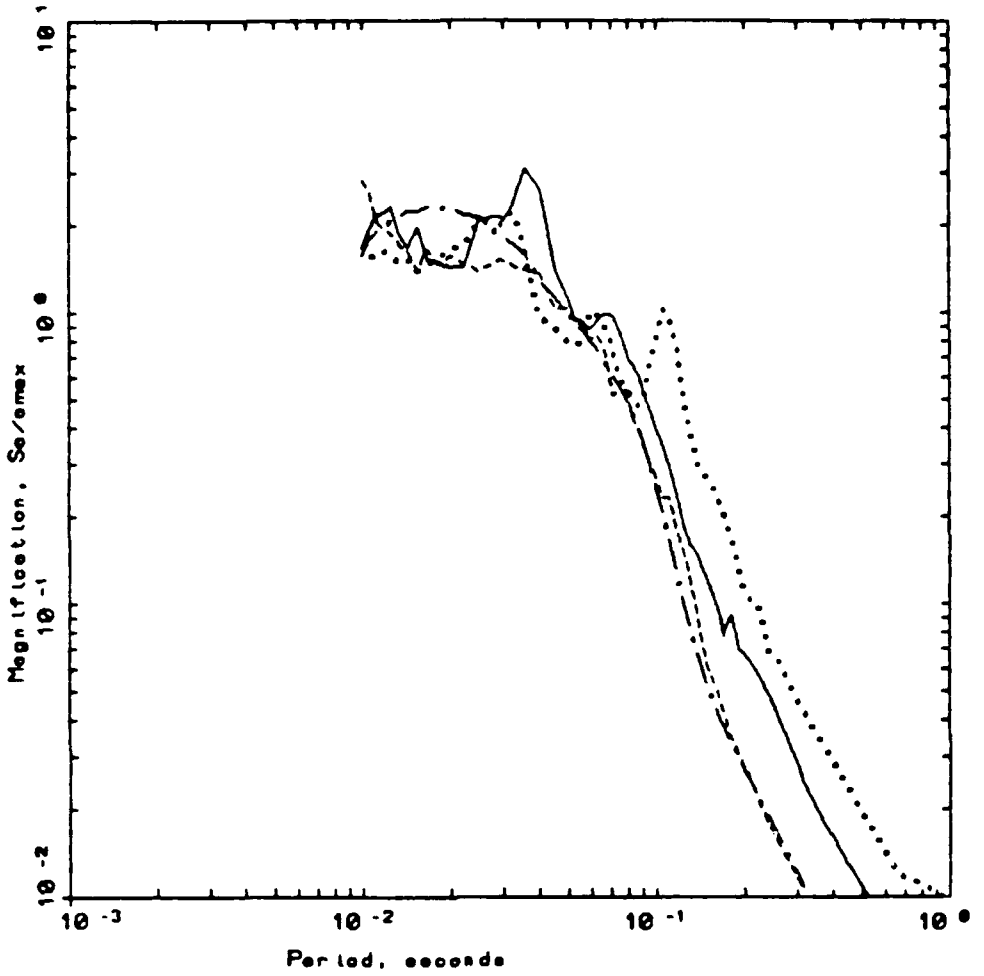

Figure 12 - Comparison of 5% response spectral shapes for the accelerograms in Figure 11. The WES-Rascal RVT estimate is the dashed - dot curves. The BLWN Fourier amplitude spectral estimate combined with the phase of an observed accelerogram is the dashed line (Spectrum 1). The 5% response spectral shapes of the recorded ground accelerations are the solid line (Spectrum 2) and the dotted line (Spectrum 3) for M_w = 2.5 at a distance of 10 km.

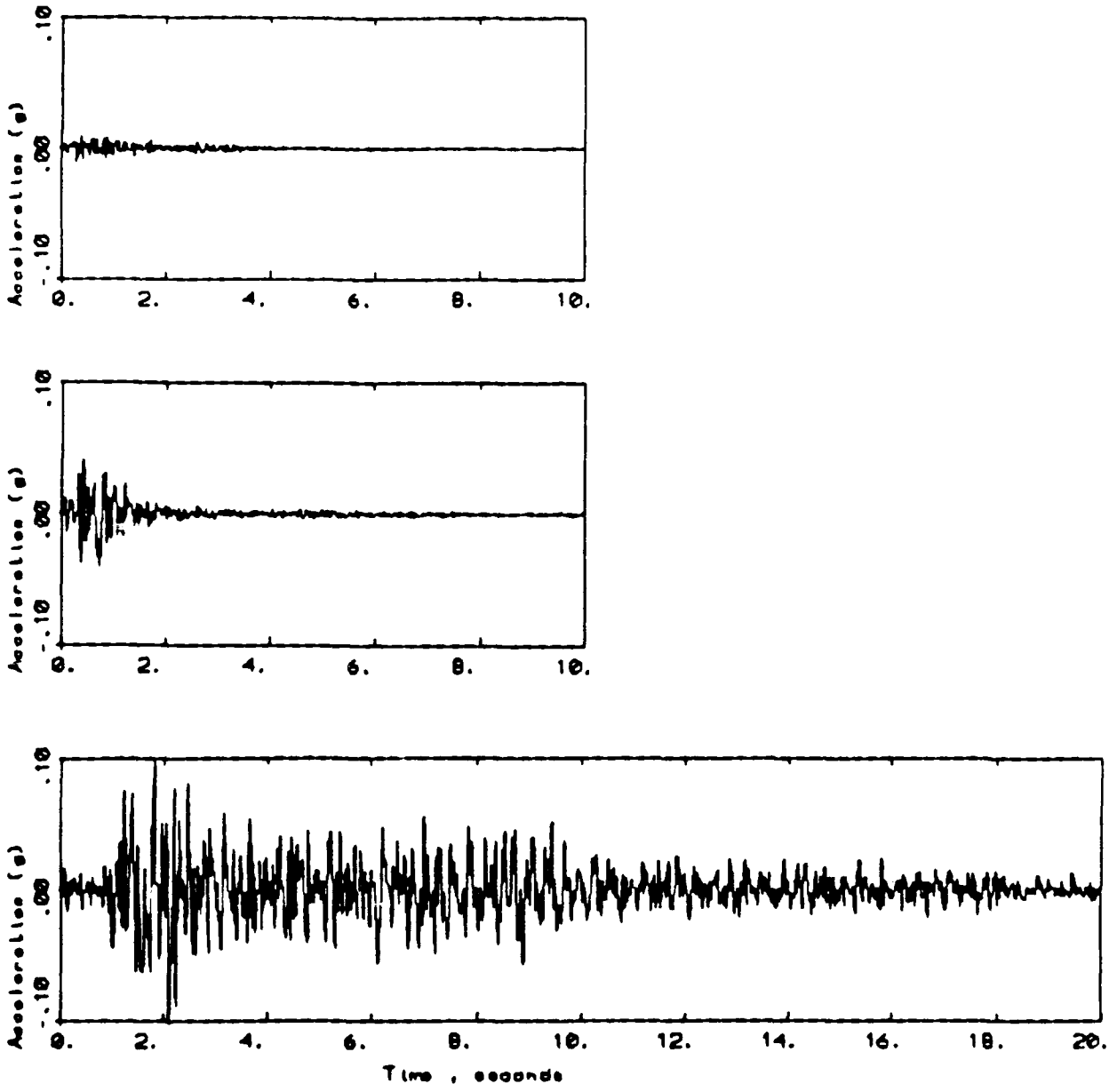

Figure 13 - Synthetic acceleration time histories(M_W = 3.0, top; M_W = 4.0 middle; M_W = 5.0, bottom) generated by adding the phase spectrum from a recorded accelerogram to the BLWN amplitude spectrum for moment magnitude (M_W) 3.0, 4.0, and 5.0 earthquakes at a distance of 10 km. WNA parameters (Table 1) are used.

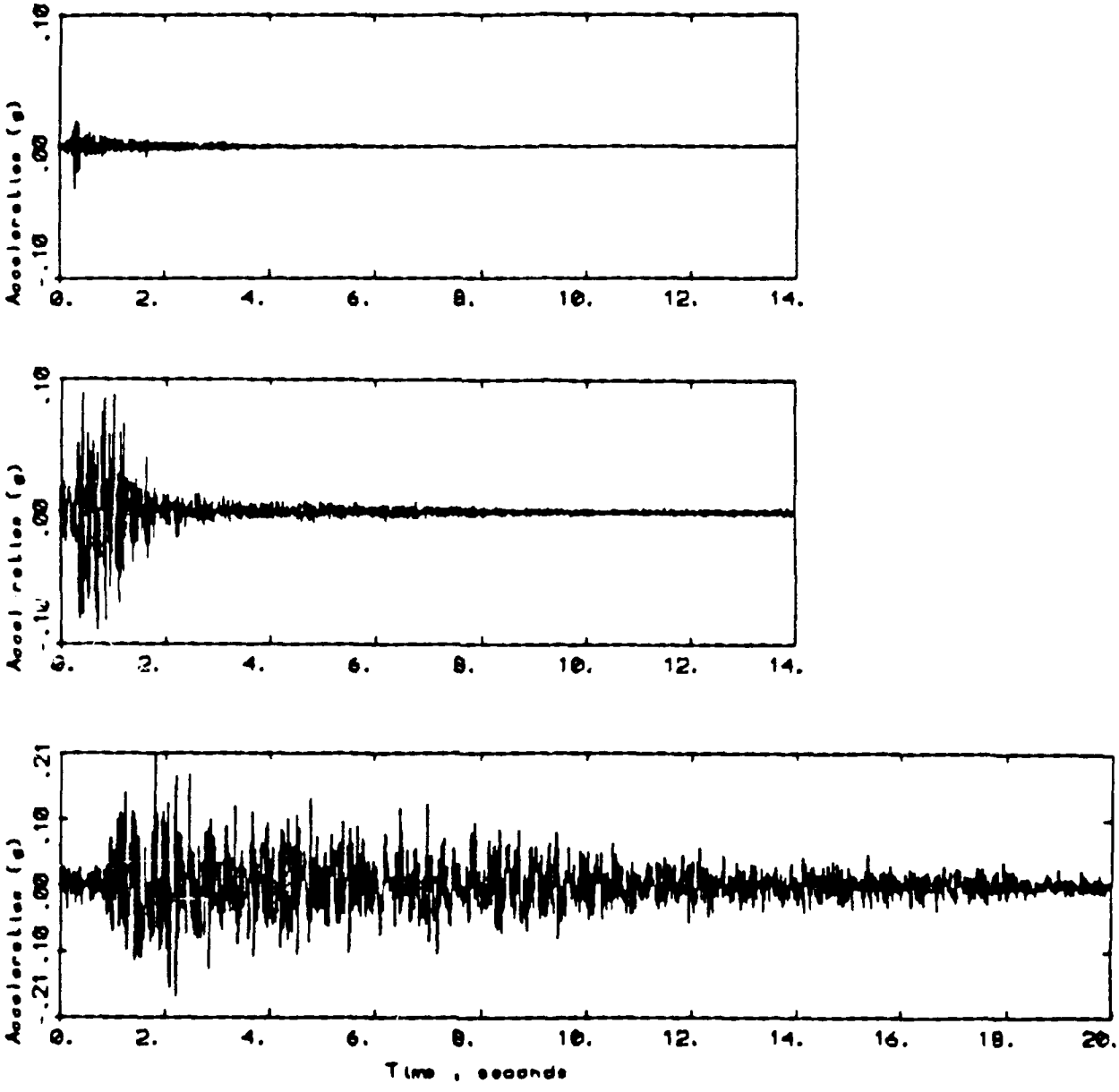

Figure 14 - Synthetic acceleration time histories (M_w = 3.0, top; M_w = 4.0, middle; M_w = 5.0, bottom) generated by adding the phase spectrum from a recorded accelerogram to the BLWN amplitude spectrum for moment magnitude (M_w) 3.0, 4.0, and 5.0 earthquakes at a distance of 10 km. ENA parameters (Table 1) are used.

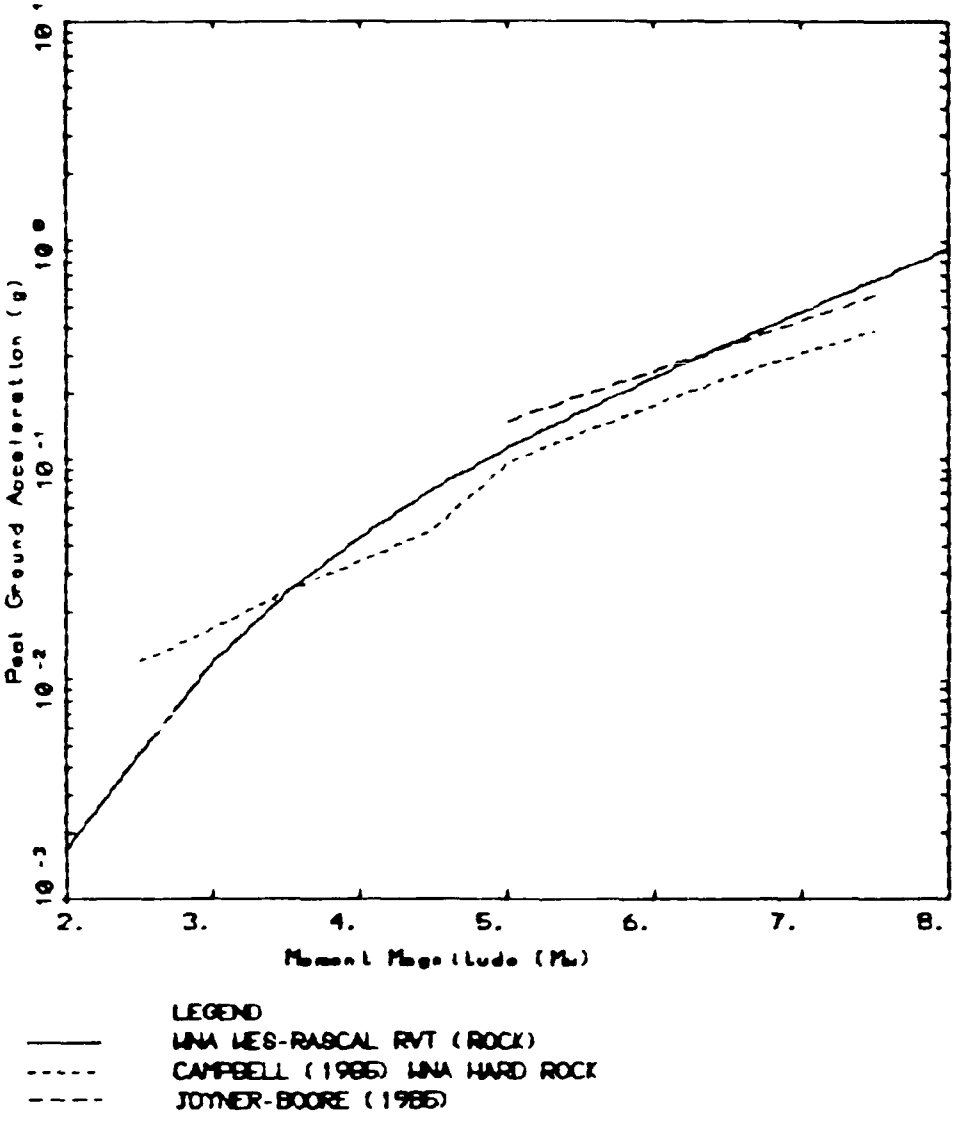

Figure 15a - WNA magnitude scaling of peak acceleration at a distance of 10 km compared to empirical predictions. BLWN RVT predictions using WNA parameters listed in Table 1 (solid line). Campbell's (1985) relation for magnitudes 2.5 - 7.5 for hard rock (short-dashed line). Joyner-Boore (in Joyner and Fumal, 1985) relation for magnitudes 5.0 - 7.5 (long-dashed line).

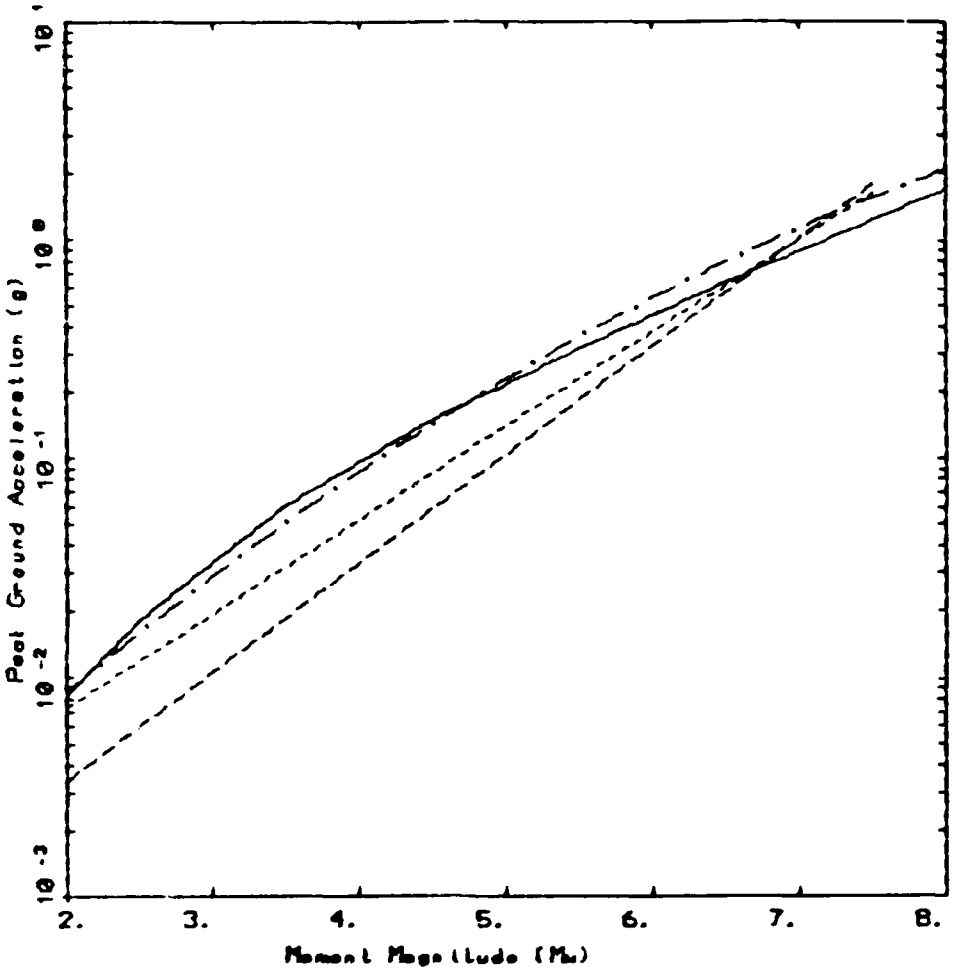

Figure 15b - ENA magnitude scaling of peak acceleration at a distance of 10 km compared to results of regressions upon RVT predicitons as well as a semi-theoretical relation. BLWN RVT predictions using ENA parameters listed in Table 1 (solid line). Regressions upon RVT predictions: Toro and McGuire (1987) (short-dashed line); Boore and Atkinson (1985) (dashed-dotted line). Nuttli et al (1986) semi-empirical relation for South Carolina (long-dashed line).

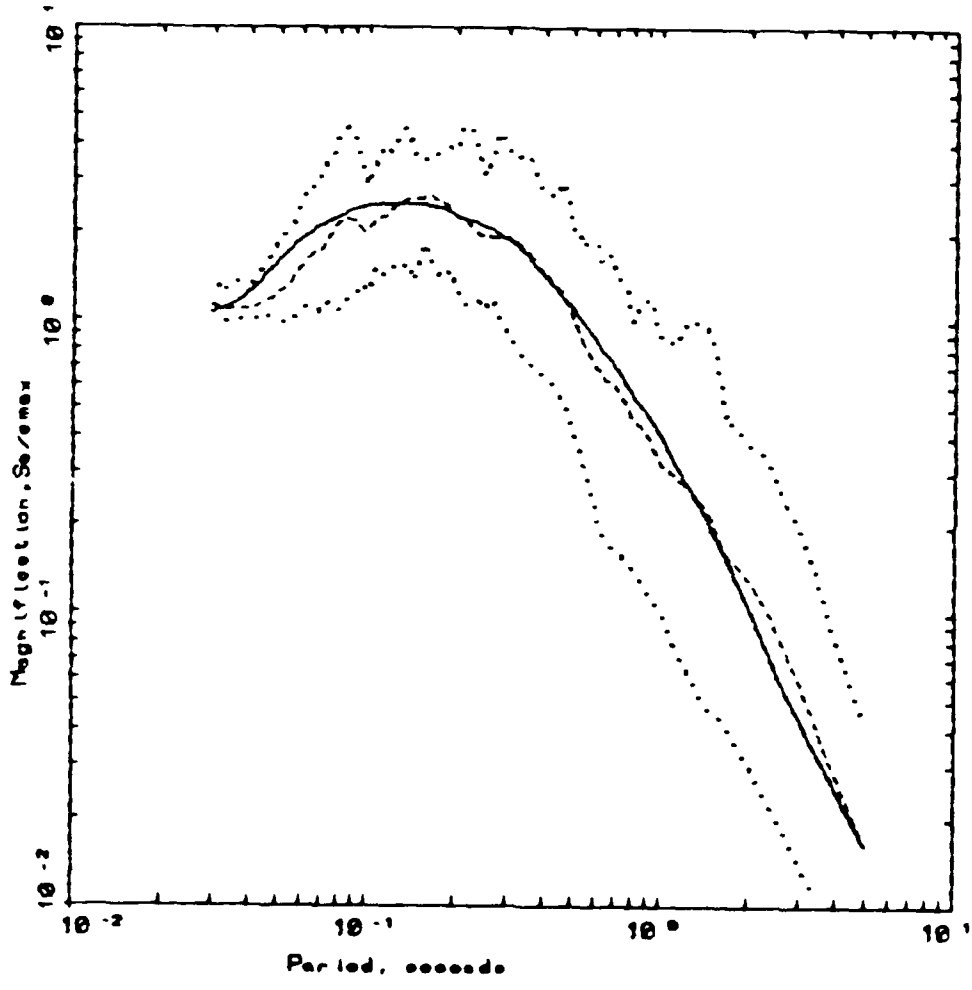

Figure 16 - Comparison of predicted response spectral shape (solid line) for a moment magnitude (M_W) 5.3 earthquake at a distance of 25 km using WNA parameters (Table 1) with average shape computed from recorded data (Table 3, dashed line). The dotted lines represent the extremes of the shapes computed from the recorded data.

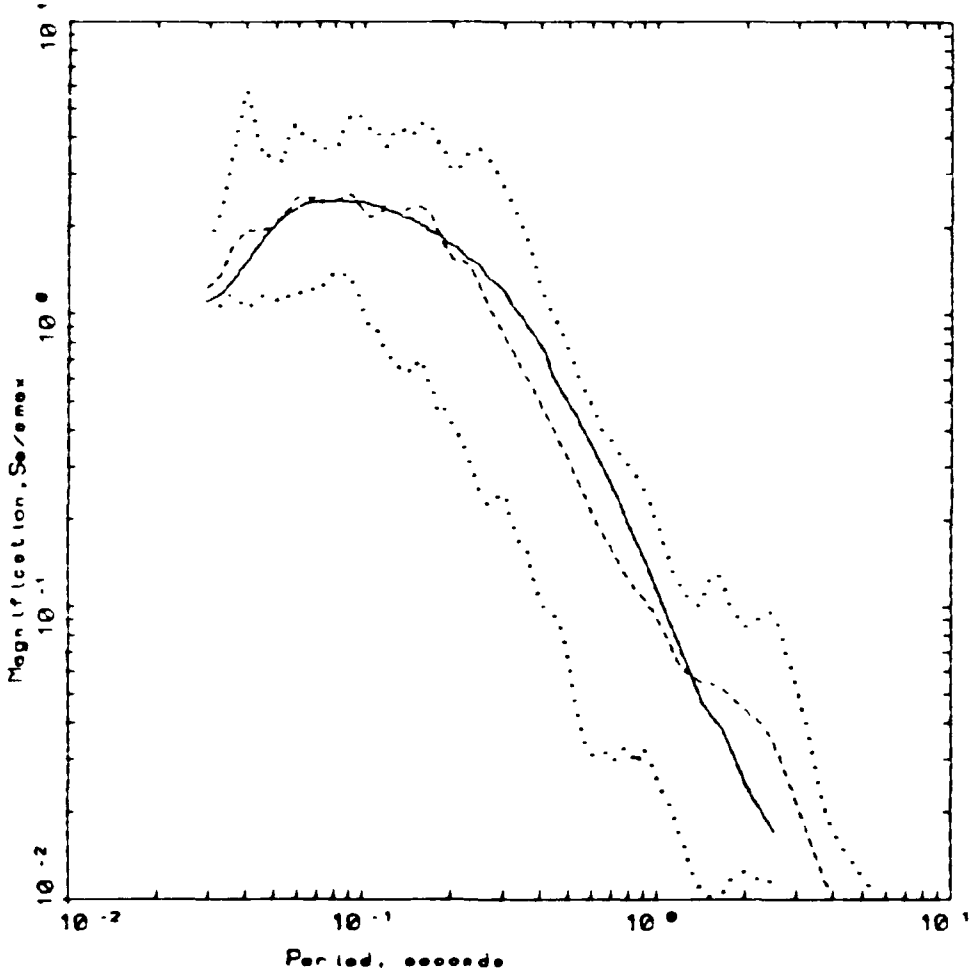

Figure 17 - Comparison of predicted response spectral shape (solid line) for a moment magnitude (M_w) 4.5 earthquake at a distance of 25 km using WNA parameters (Table 1) with average shape computed from recorded data (Table 5, dashed line). The dotted lines represent the extremes of the shapes computed from the recorded data.

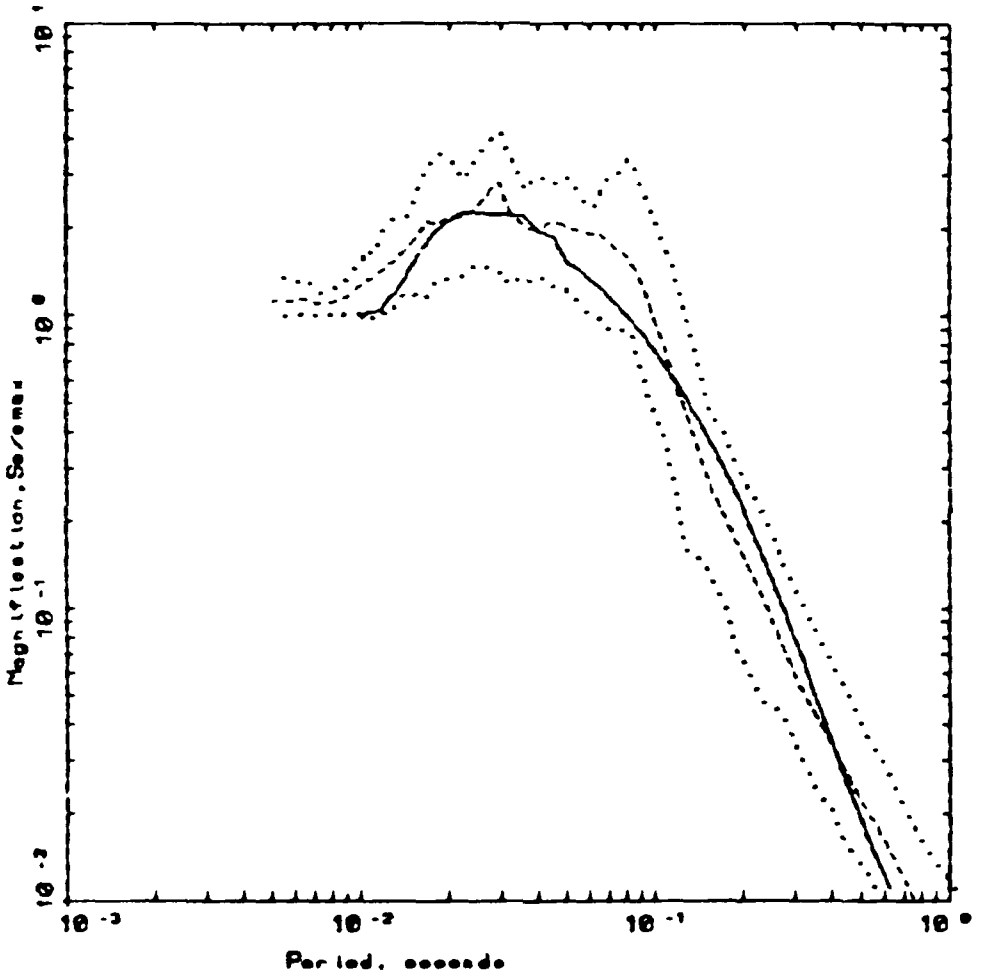

Figure 18 - Comparison of predicted response spectral shape (solid line) for a moment magnitude (M_W) 2.5 earthquake at a distance of 25 km using WNA parameters (Table 1) with average shape computed from recorded data (Table 7, dashed line). The dotted lines represent the extremes of the shapes computed from the recorded data.

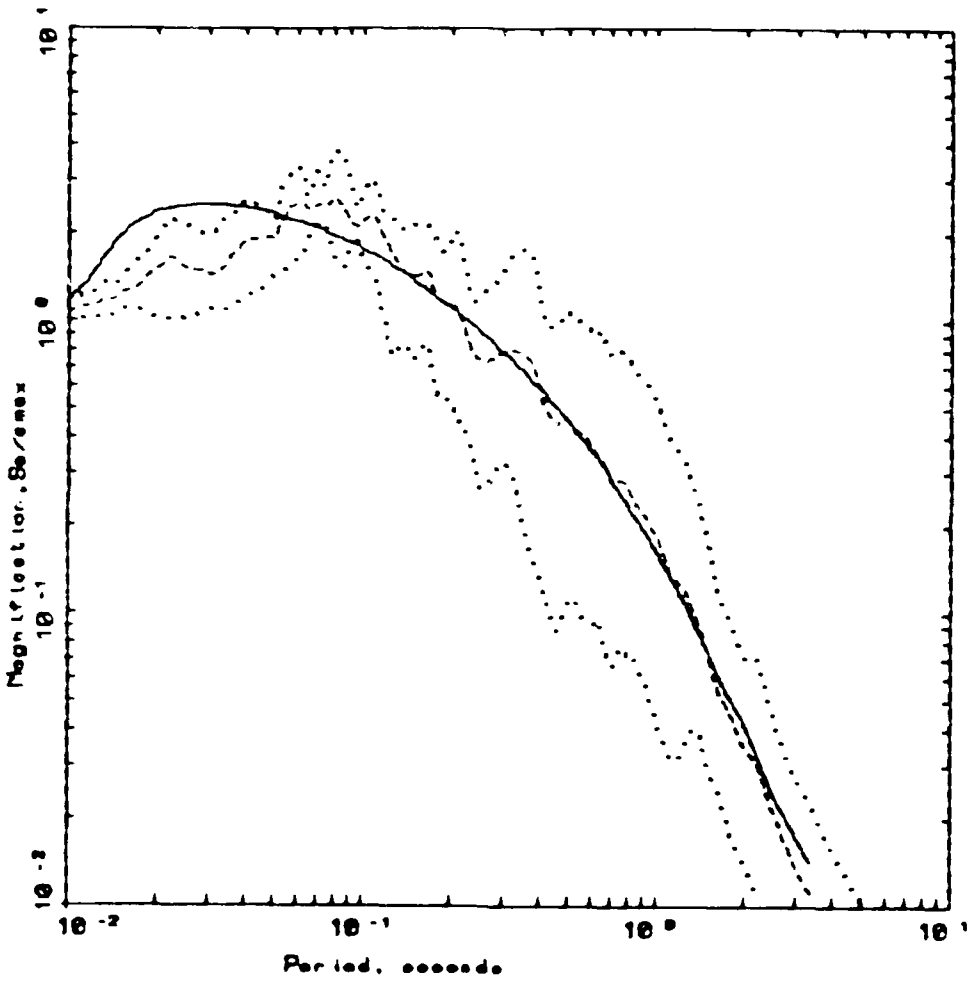

Figure 19 - Comparison of predicted response spectral shape (solid line) for a moment magnitude (M_w) 5.3 earthquake at a distance of 25 km using ENA parameters (Table 1) with average shape computed from recorded data (Table 4, dashed line). The dotted lines represent the extremes of the shapes computed from the recorded data.

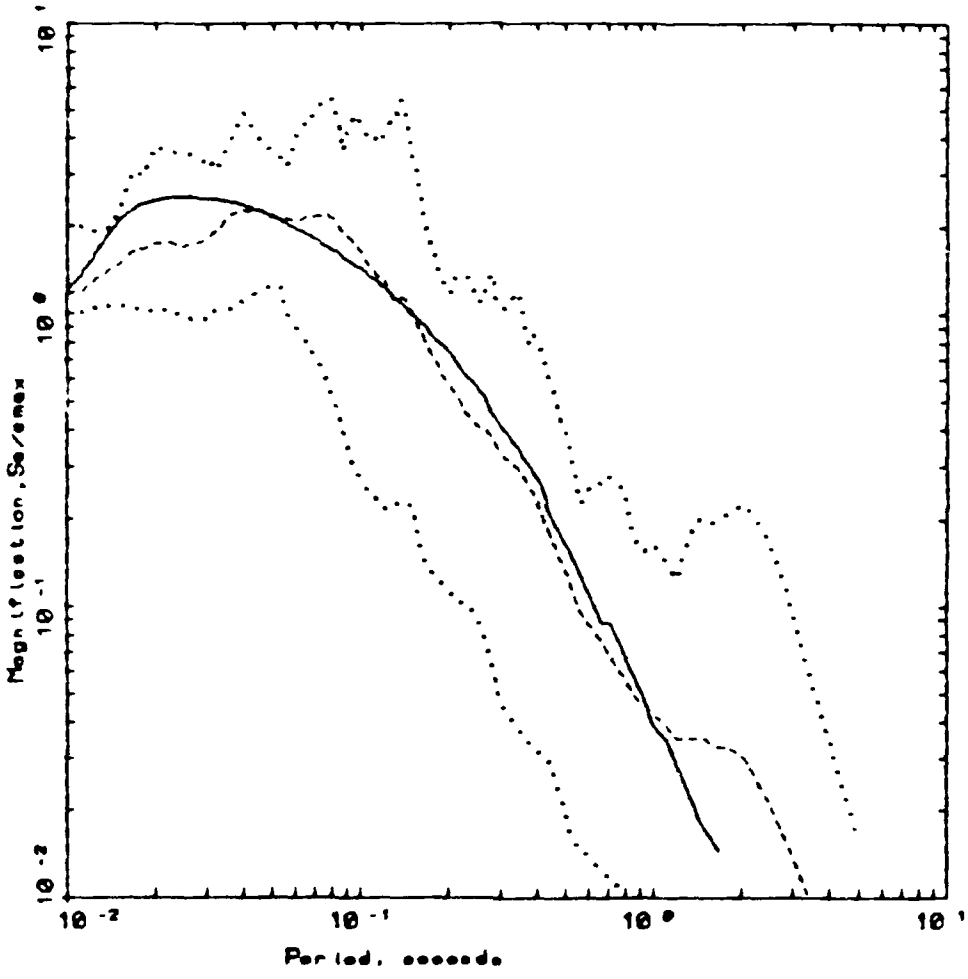

Figure 20 - Comparison of predicted response spectral shape (solid line) for a moment magnitude (M_w) 4.5 earthquake at a distance of 8 km using ENA parameters (Table 1) with average shape computed from recorded data (Table 6, dashed line). The dotted lines represent the extremes of the shapes computed from the recorded data.

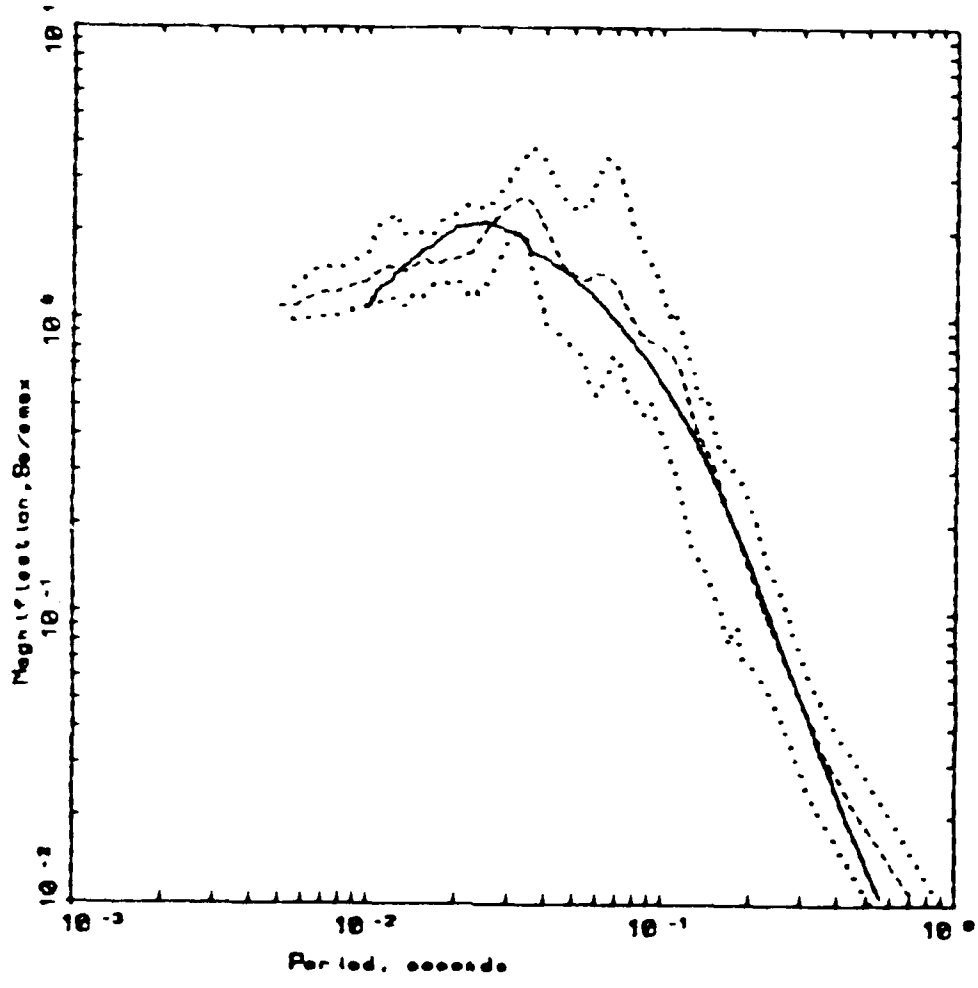

Figure 21 - Comparison of predicted response spectral shape (solid line) for a moment magnitude (M_w) 2.5 earthquake at a distance of 10 km using WNA parameters (Table 1) with average shape computed from recorded data (Table 8, dashed line). The dotted lines represent the extremes of the shapes computed from the recorded data.

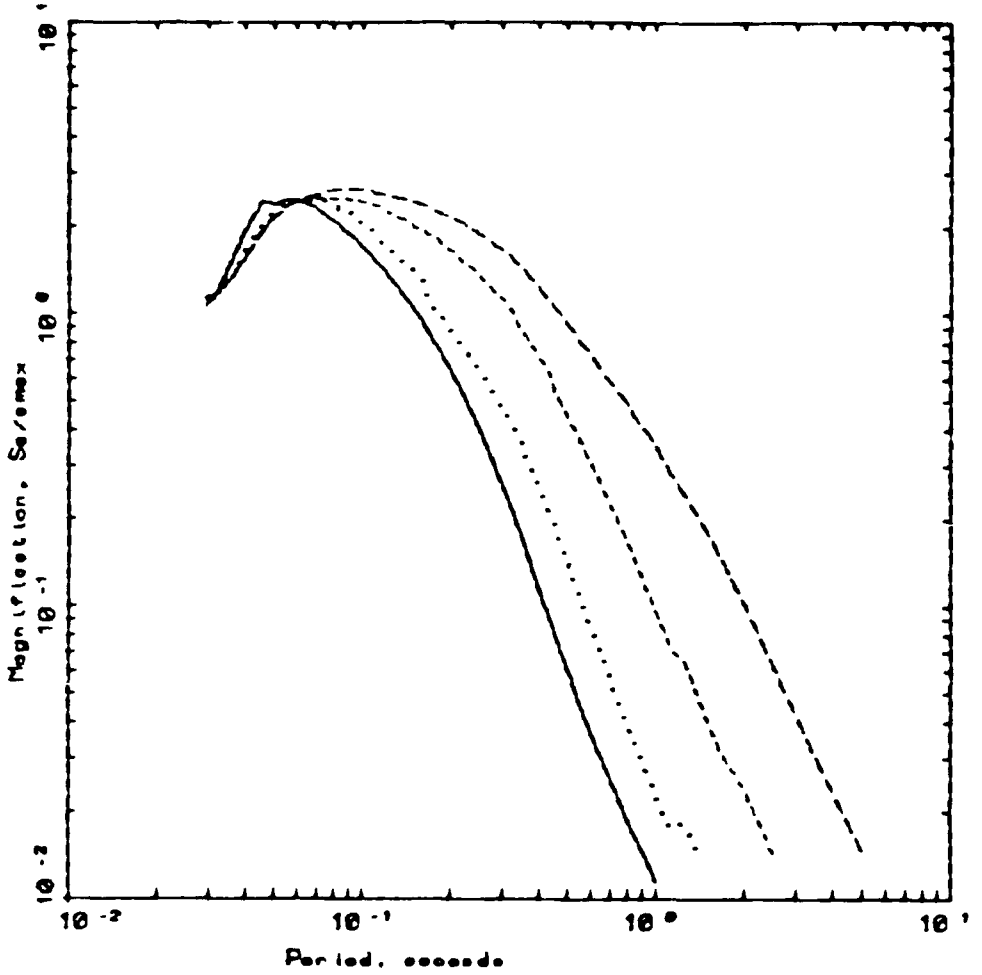

Figure 22 - Effect of moment magnitude (M_w) upon response spectral shapes using WNA parameters (Table 1) at a hypocentral distance of 10 km.

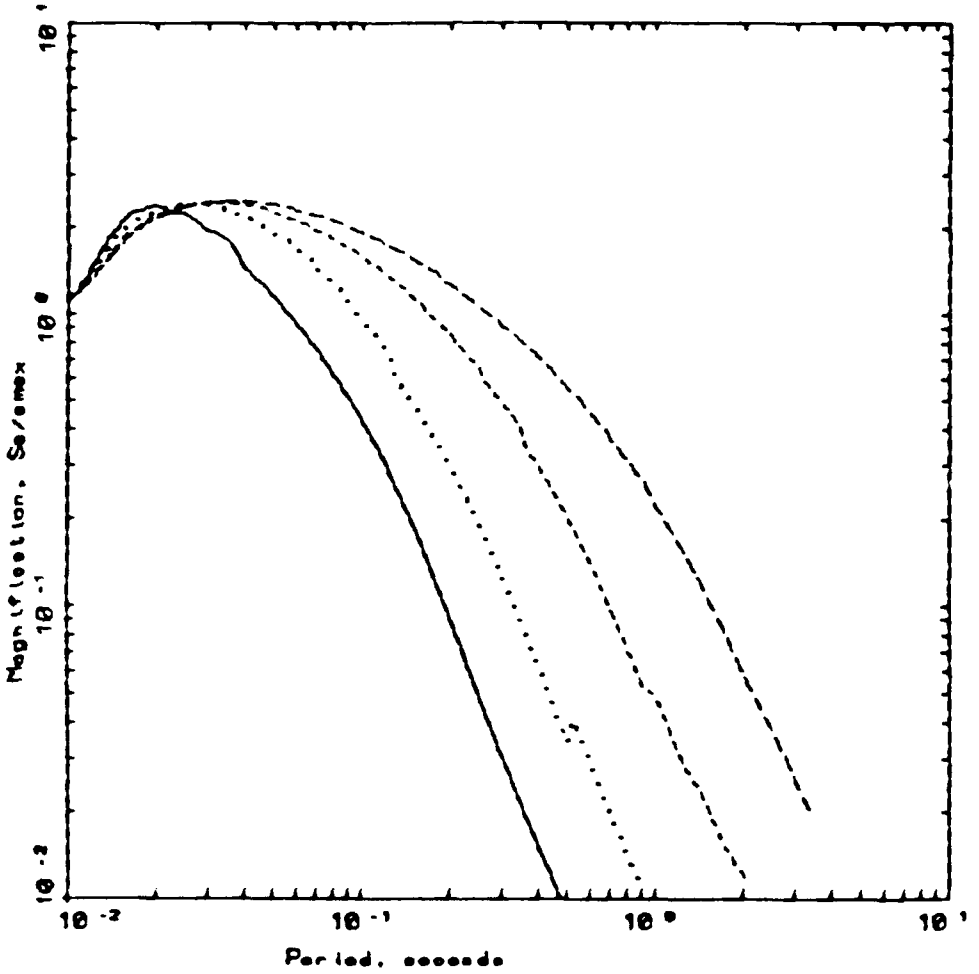

Figure 23 - Effect of moment magnitude (M_w) upon response spectral shapes using ENA parameters (Table 1) at a hypocentral distance of 10 km.

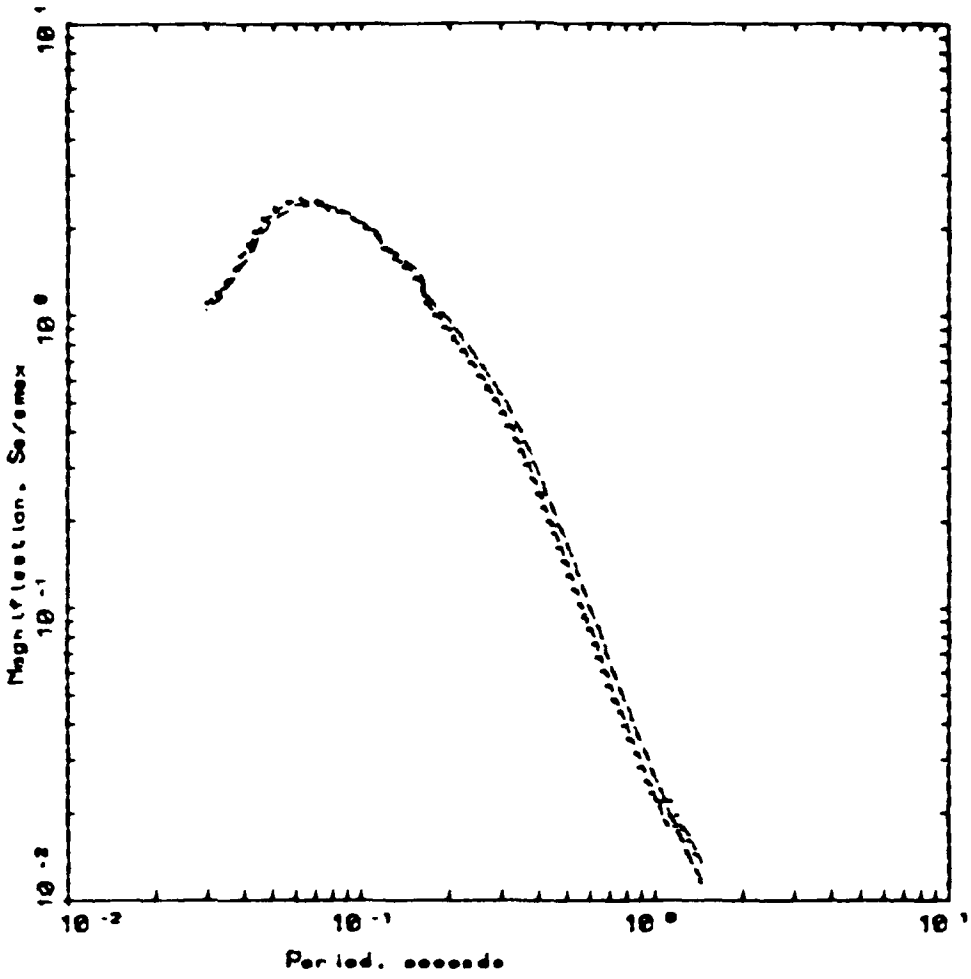

Figure 24 - Effect of distance upon absolute acceleration response spectral shape for a moment magnitude (M_w) 3.5 earthquake using WNA parameters (Table 1).

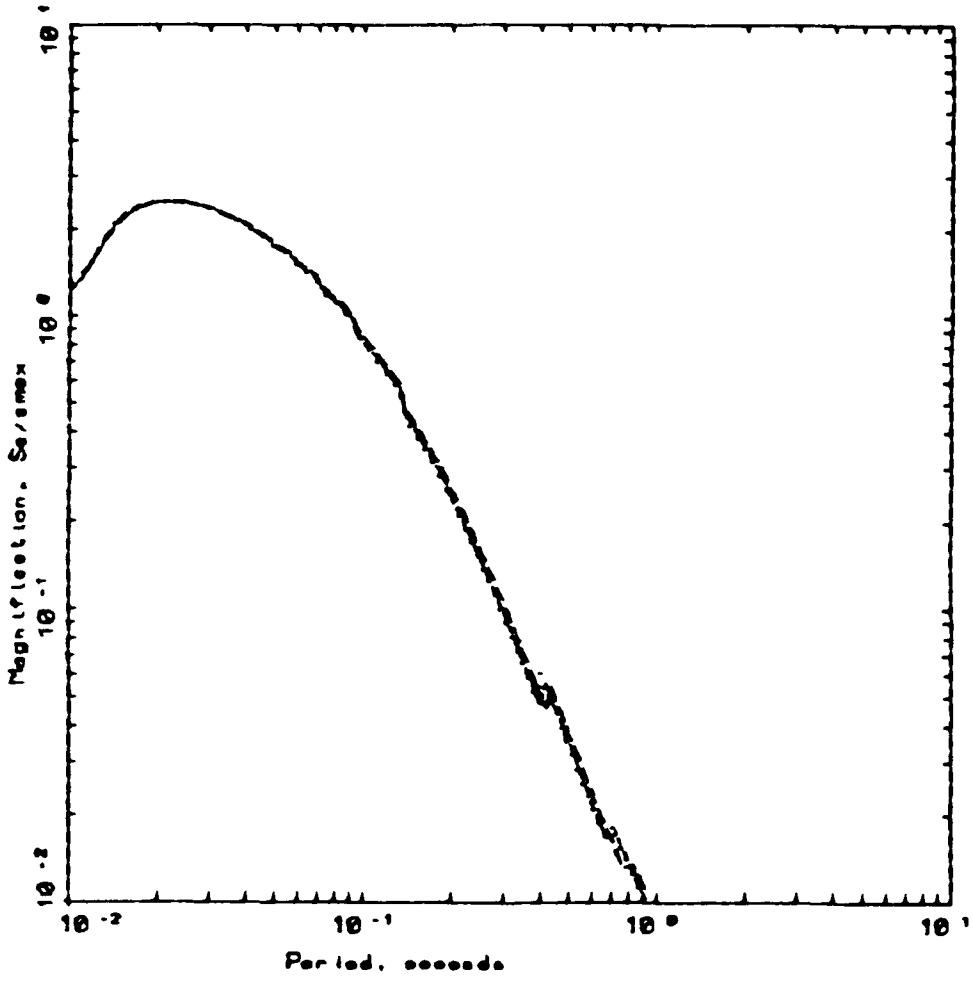

Figure 25 - Effect of distance upon absolute acceleration reponse spectral shape for a moment magnitude (M_w) 3.5 earthquake using ENA parameters (Table 1).

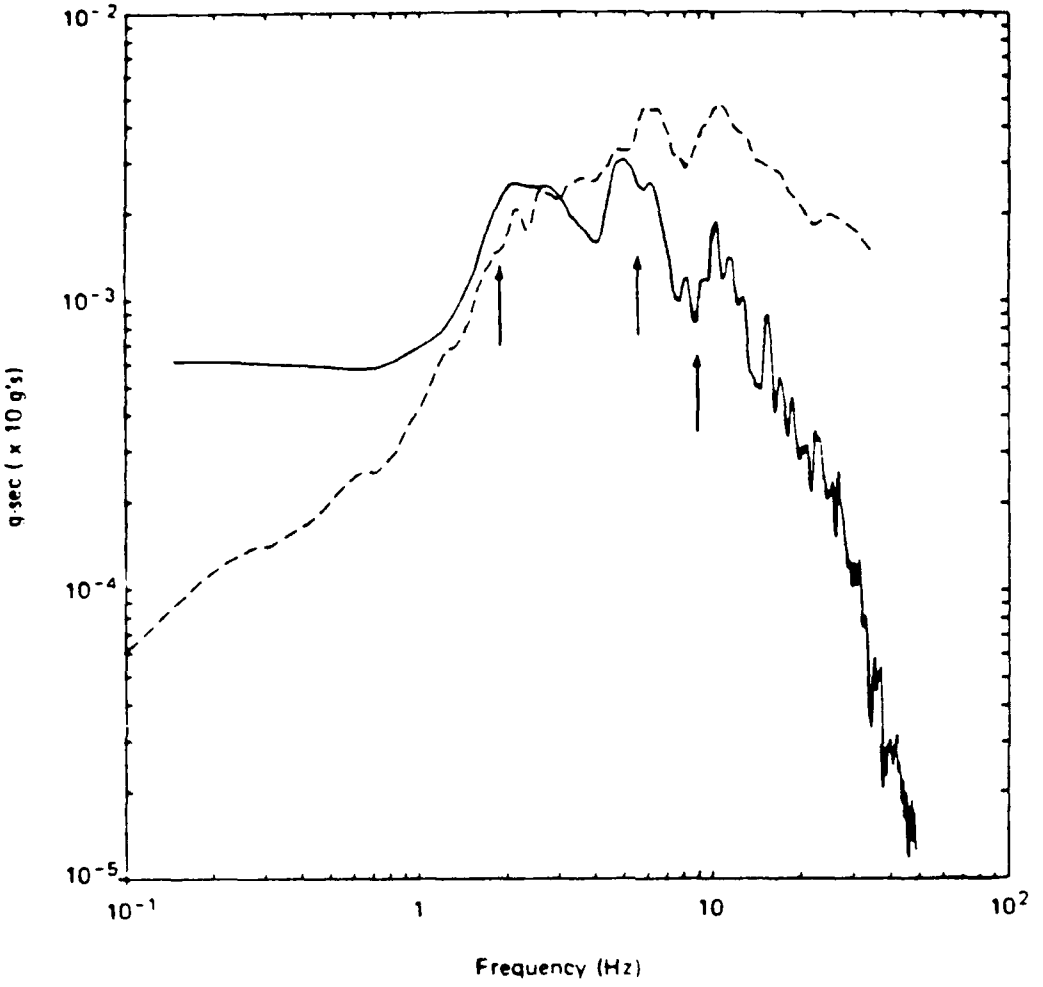

Figure 26 - Response spectra and Fourier spectra for data recorded at the Richmond Field Station vertical array from the Briones Hills(M_L = 4.3) Earthquake. Accelerometers are at depths 0, 15m, and 40m (bedrock). The solid line is the geometrical mean of the Fourier spectral density for the two horizontal components. A 1 Hz wide triangular operator has been applied prior to taking the mean. The dashed line is the geometrical mean of the 5% absolute acceleration response spectra. The plot represents surface data.

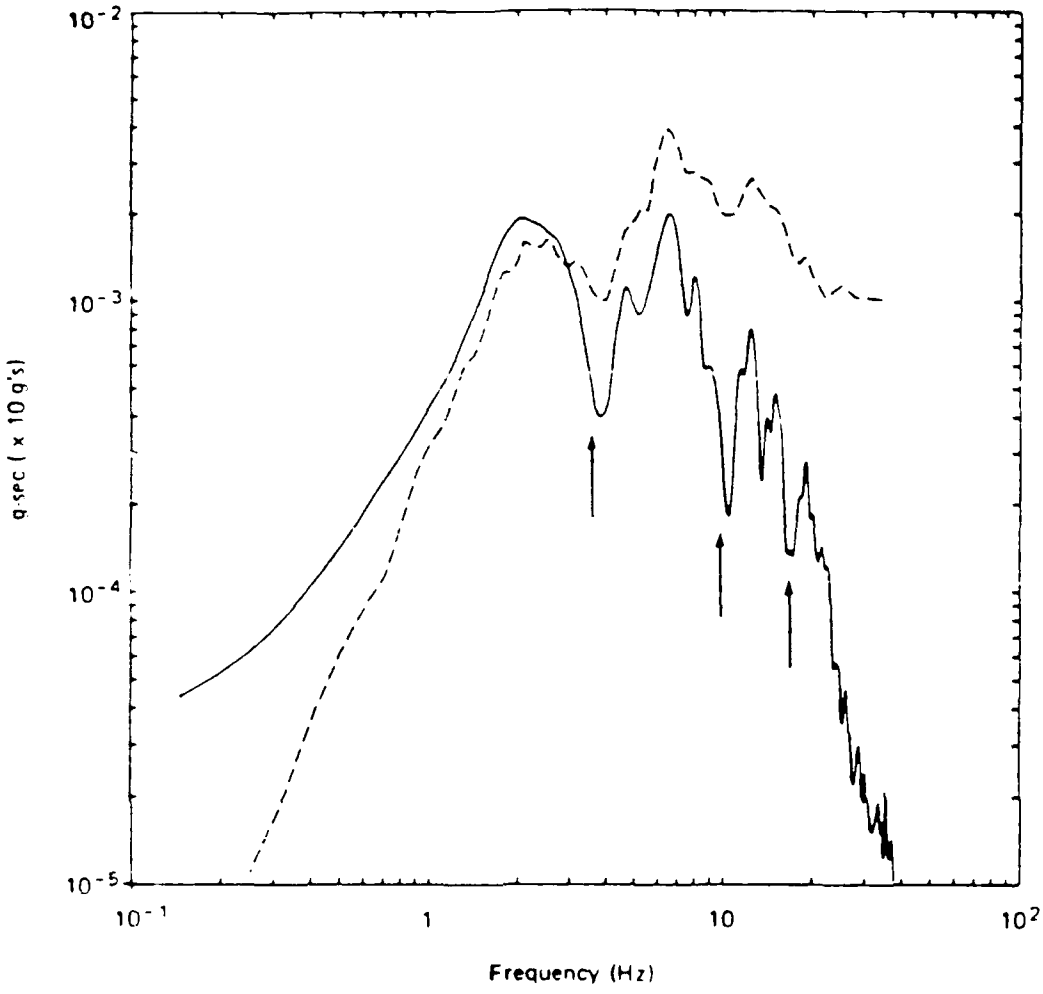

Figure 27 - Response spectra and Fourier spectra for data recorded at the Richmond Field Station vertical array from the Briones Hills (M_L = 4.3) Earthquake. Accelerometers are at depths 0, 15m, and 40m (bedrock). The solid line is the geometrical mean of the Fourier spectral density for the two horizontal components. A 1 Hz wide triangular averaging operator has been applied prior to taking the mean. The dashed line is the geometrical mean of the 5% absolute acceleration response spectra. The plot represents mid-hole data.

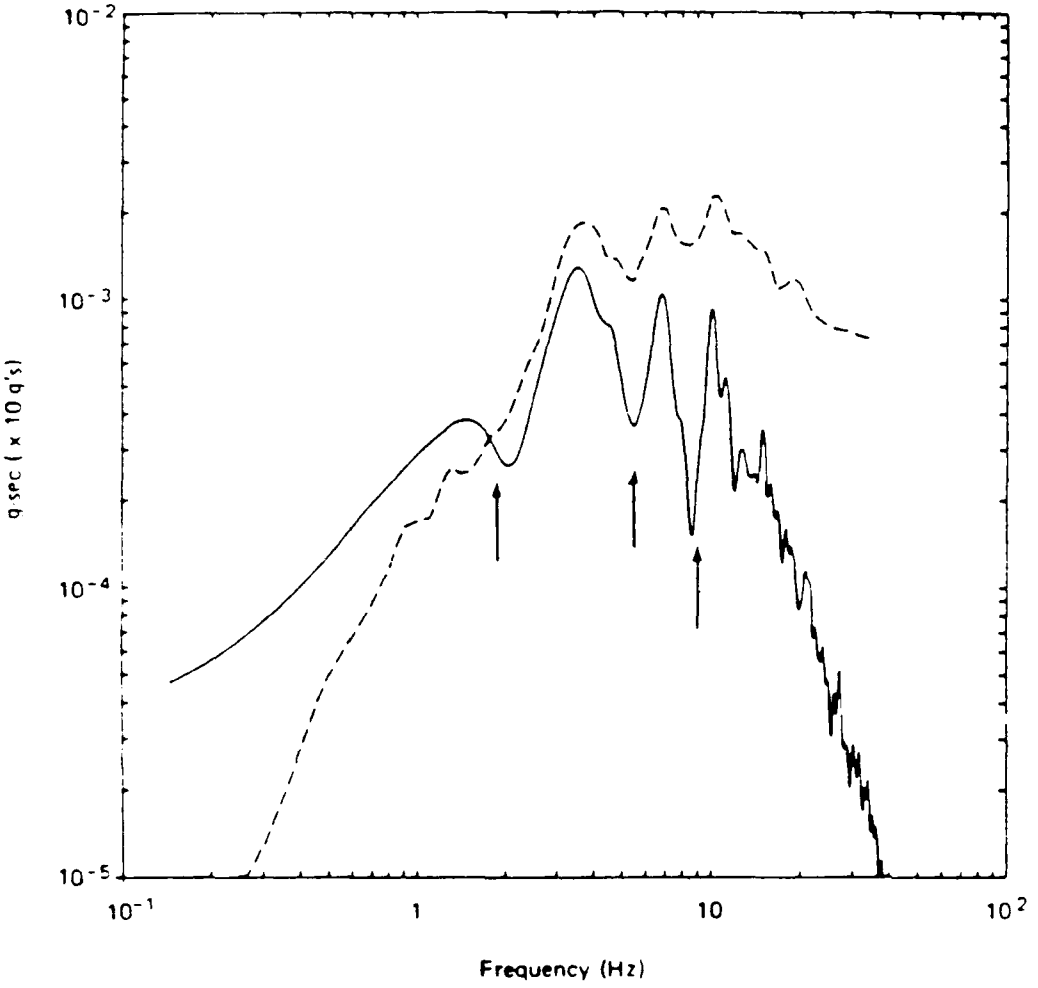

RICHMOND FIELD STATION
BRIONES HILLS EQ. (M_L = 4.3)

LEGEND

——— Bottom Mean Horizontal Fourier Spectrum: g-sec (1 Hz Smoothing Window)

– – – – Bottom Mean Horizontal Absolute Acceleration: x 10 g's (5% Damping)

Figure 28 - Response spectra and Fourier spectra for data recorded at the Richmond Field Station vertical array from the Briones Hills (M_L = 4.3) Earthquake. Accelerometers are at depths 0, 15m, and 40m (bedrock). The solid line is the geometrical mean of the Fourier spectral density for the two horizontal components. A 1 Hz wide triangular averaging operator has been applied prior to taking the mean. The dashed line is the geometrical mean of the 5% absolute acceleration response spectra. The plot represents bedrock data.

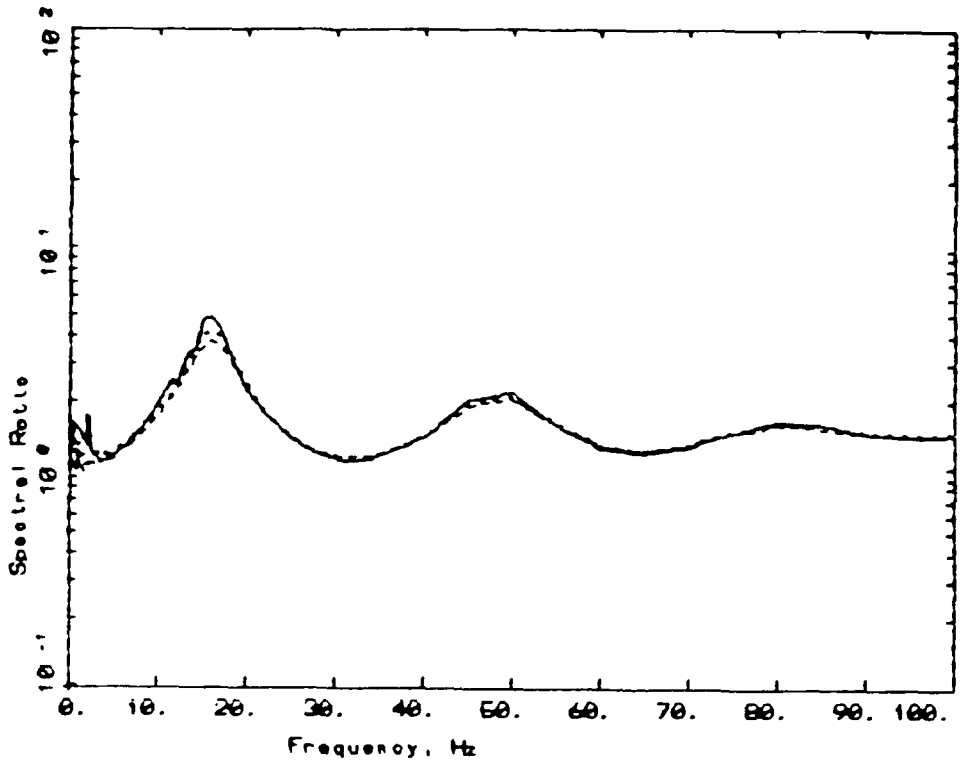

RESPONSE SPECTRAL RATIO

LEGEND

5 %, Spectral Ratio between 0 and 50m (Mw=3)

5 %, Spectral Ratio between 0 and 50m (Mw=4)

5 %, Spectral Ratio between 0 and 50m (Mw=5)

Figure 29 - Response spectral ratios between the surface and 50 m depth within a halfspace. Moment magnitudes range from 3 to 5 and the synthetics are representative of a hypocentral range of 5 km and eastern United States parameters (Table 1).

The offsets shown in the response spectra plots are due to changes in the estimated number of zero crossings in the oscillator response. The number of zero crossings (or extrema) is proportional to the ratio between the peak value and the RMS of the oscillator response.

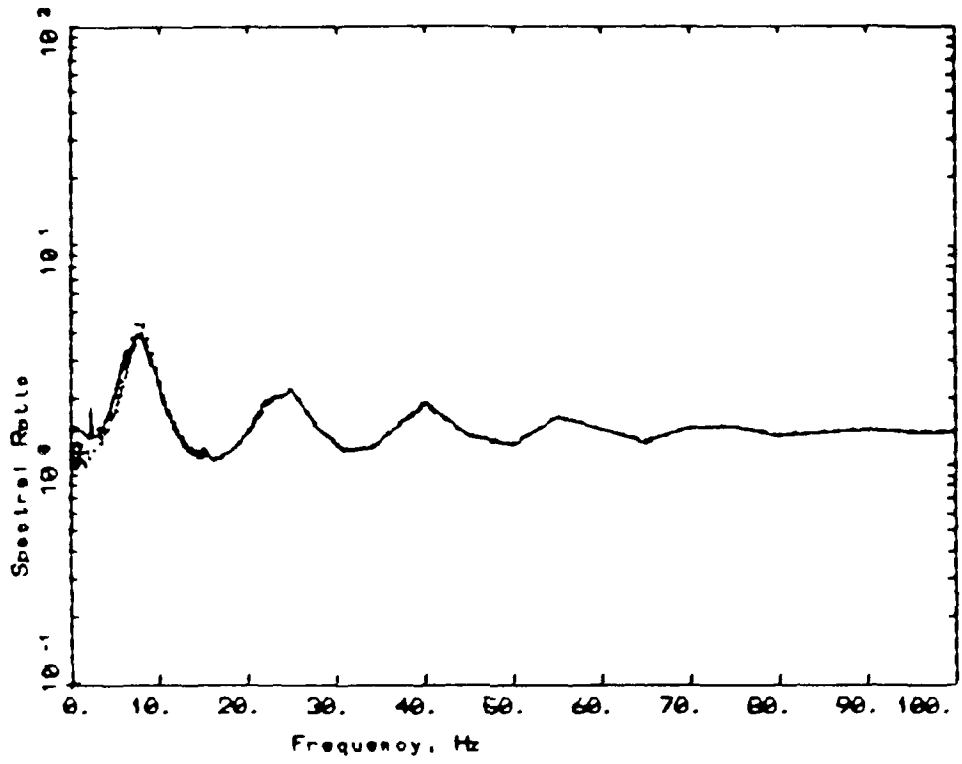

RESPONSE SPECTRAL RATIO

LEGEND

5 %, Spectral Ratio between 0 and 100m (Mw=3)

5 %, Spectral Ratio between 0 and 100m (Mw=4)

5 %, Spectral Ratio between 0 and 100m (Mw=5)

Figure 30 - Response spectral ratios between the surface and 100 m depth within a halfspace. Moment magnitudes range from 3 to 5 and the synthetics are representative of a hypocentral range of 5 km and eastern United States parameters (Table 1).

The offsets shown in the response spectra plots are due to changes in the estimated number of zero crossings in the oscillator response. The number of zero crossings (or extrema) is proportional to the ratio between the peak value and the RMS of the oscillator response.

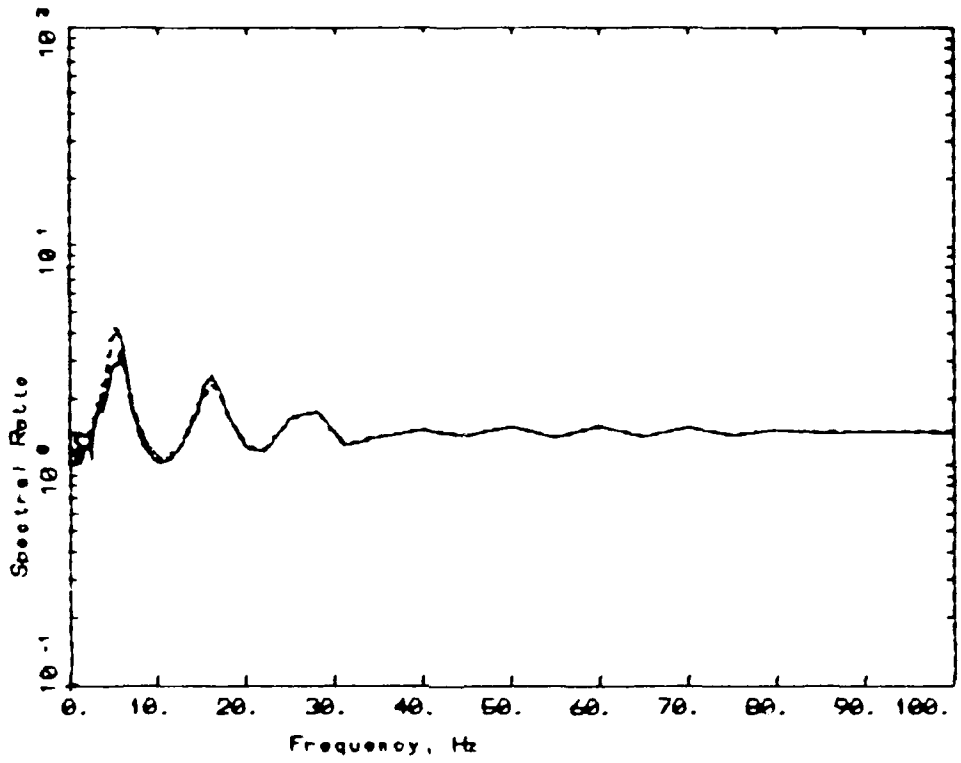

RESPONSE SPECTRAL RATIO

LEGEND

5 %, Spectral Ratio between 0 and 150m (Mw=3)

6 %, Spectral Ratio between 0 and 150m (Mw=4)

6 %, Spectral Ratio between 0 and 150m (Mw=5)

Figure 31 - Response spectral ratios between the surface and 150 m depth within a halfspace. Moment magnitudes range from 3 to 5 and the synthetics are representative of a hypocentral range of 5 km and eastern United States parameters (Table 1).

The offsets shown in the response spectra plots are due to changes in the estimated number of zero crossings in the oscillator response. The number of zero crossings (or extrema) is proportional to the ratio between the peak value and the RMS of the oscillator response.

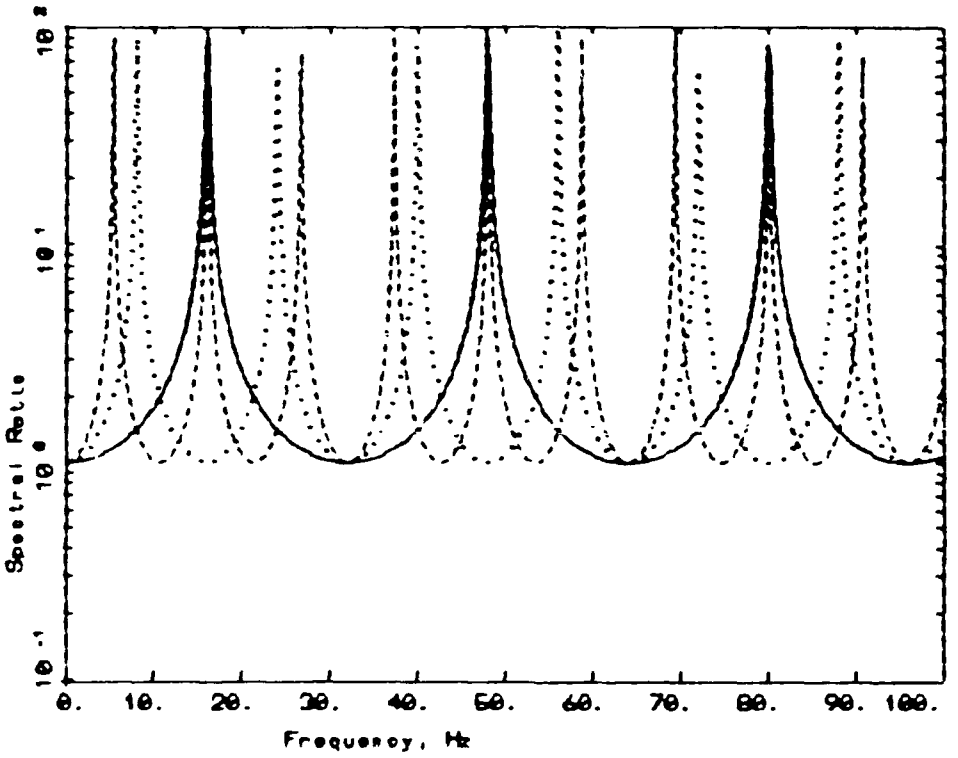

FOURIER SPECTRAL RATIO

LEGEND

5 m, Spectral Ratio between 0 and 50m (Mw=3,4,5)

6 m, Spectral Ratio between 0 and 100m (Mw=3,4,5)

5 m, Spectral Ratio between 0 and 150m (Mw=3,4,5)

Figure 32 - Fourier spectral ratios between the surface and 50, 100, and 150 m depths within a halfspace. The Fourier spectral ratio is magnitude independent. The hypocentral distance is 5 km.

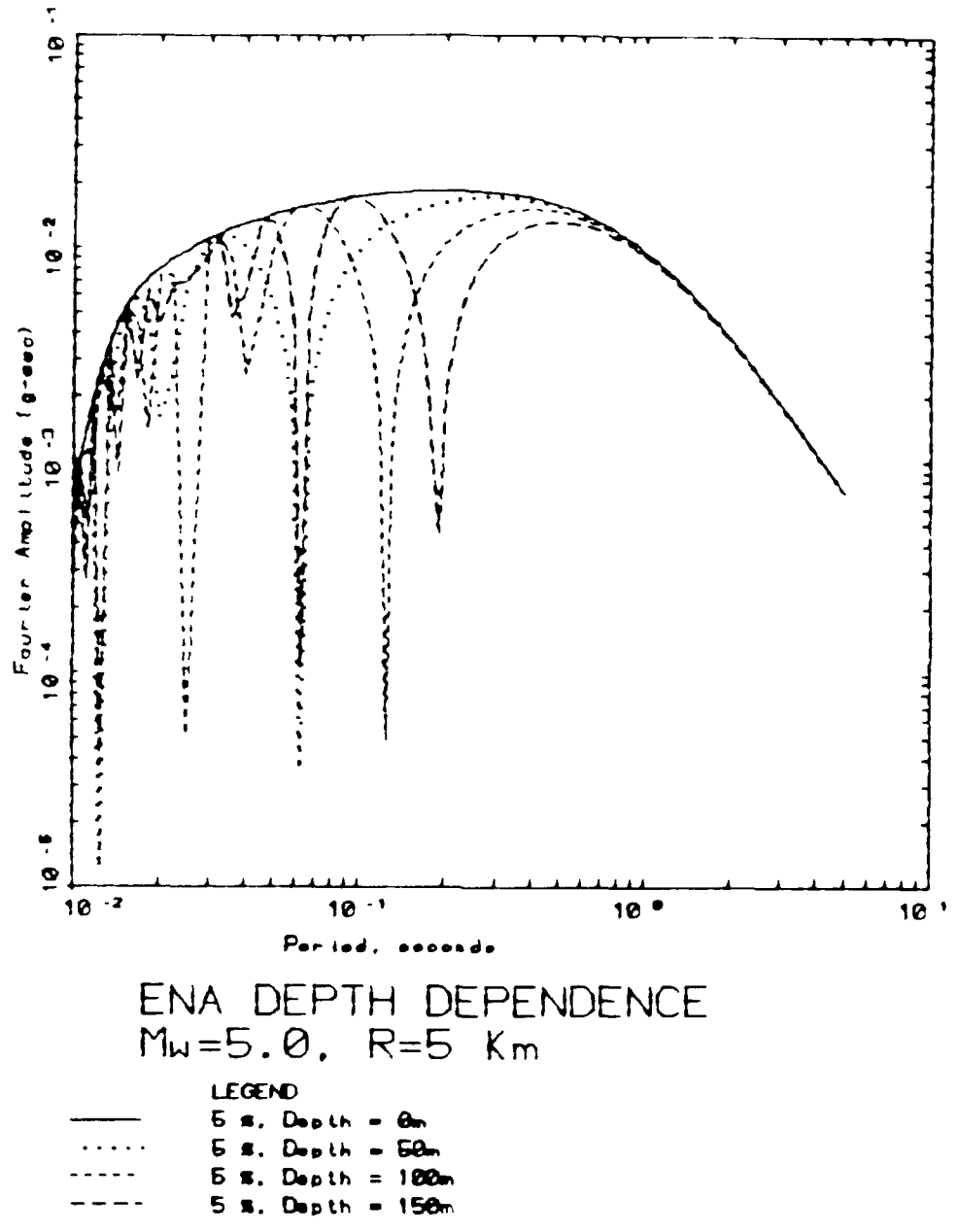

Figure 33 - Individual Fourier spectra at the surface and at depths of 50, 100, and 150 m for moment magnitude 5.0 at a hypocentral distance of 5 km.

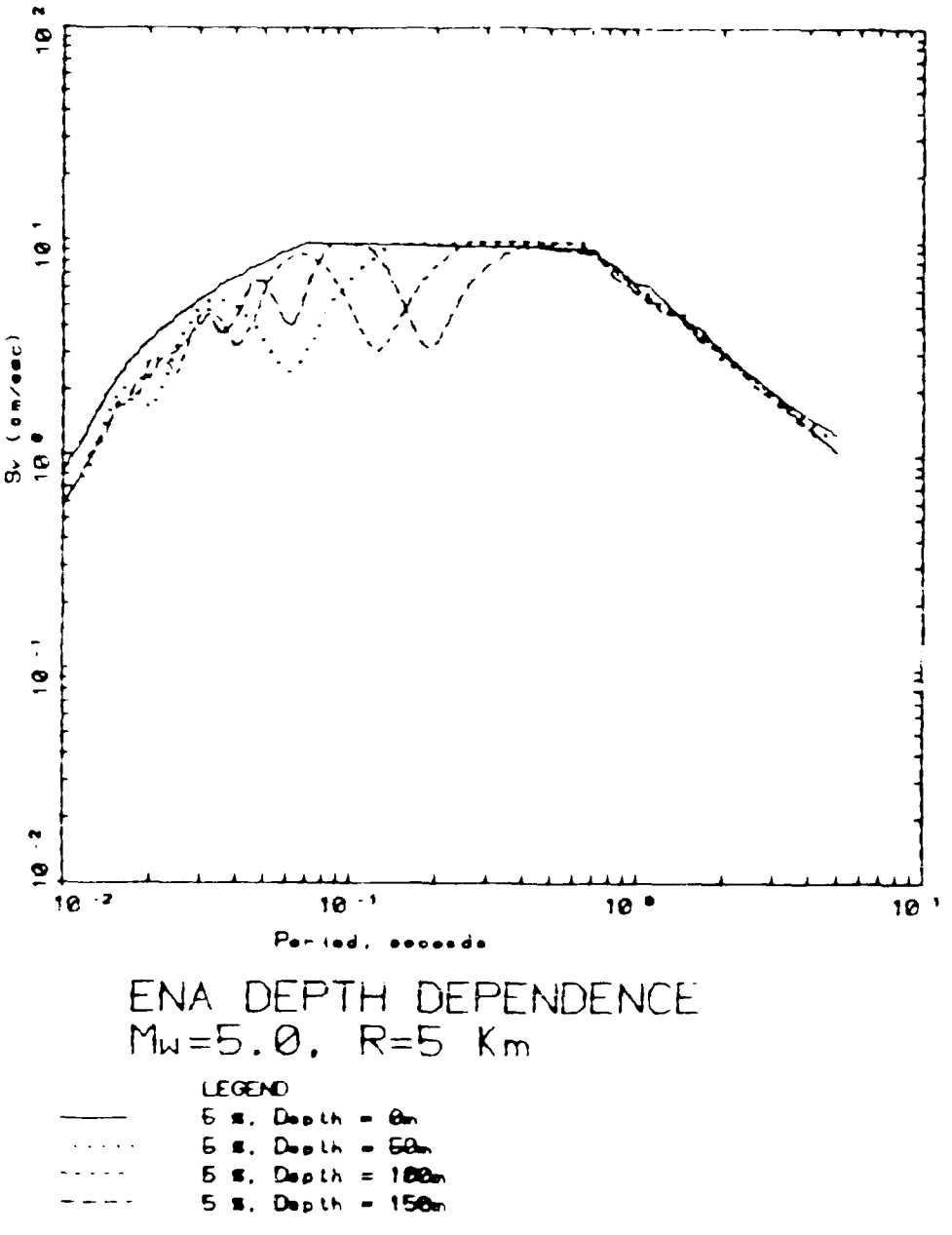

Figure 34 - Individual response spectra at the surface and at depths of 50, 100, and 150 m within a halfspace for moment magnitude 5.0 at a hypocentral distance of 5 km.

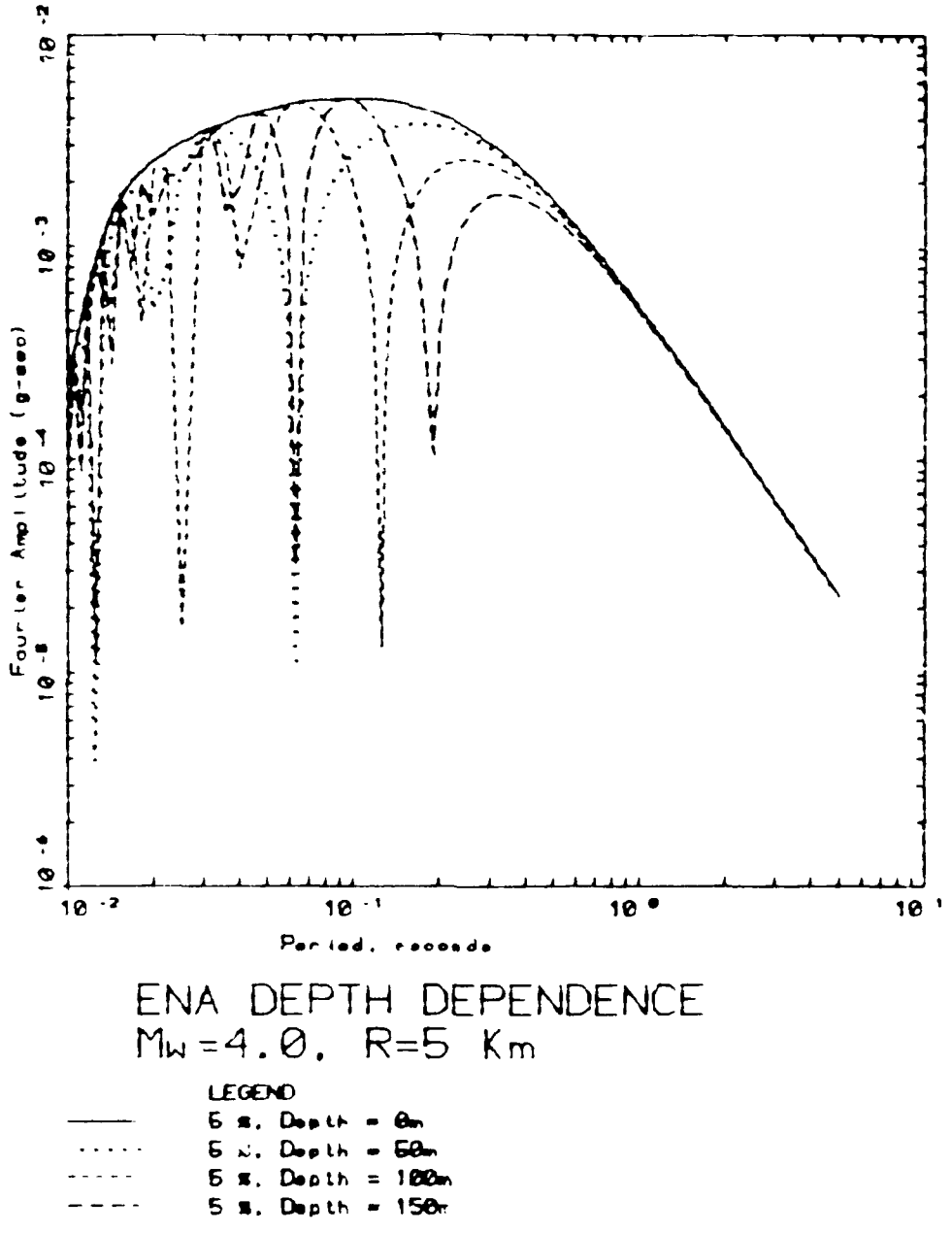

Figure 35 - Individual Fourier spectra at the surface and at depths of 50, 100, and 150 m within a halfspace for moment magnitude 4.0 at a hypocentral distance of 5 km.

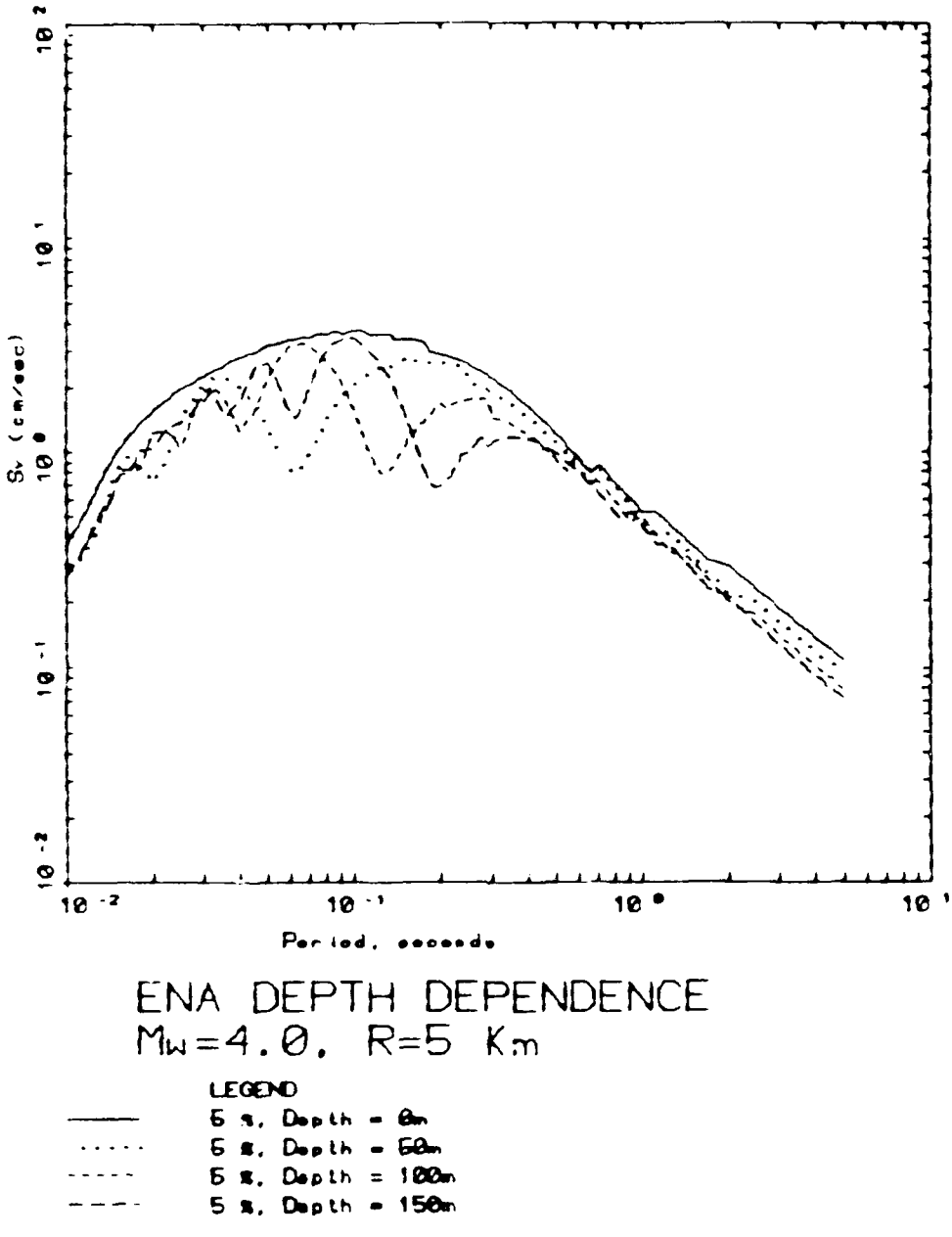

Figure 36 - Individual response spectra at the surface and at depths of 50, 100, and 150 m within a halfspace for moment magnitude 4.0 at a hypocentral distance of 5 km.

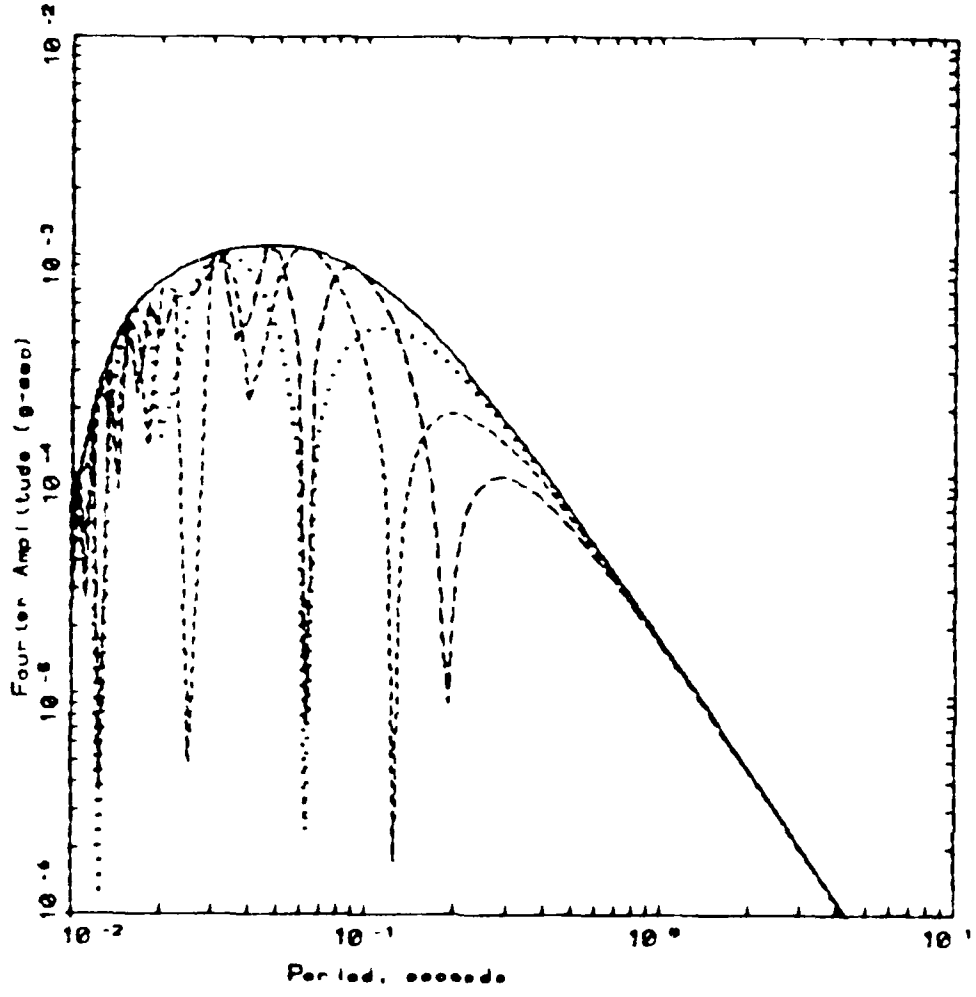

Figure 37 - Individual Fourier spectra at the surface and at depths of 50, 100, and 150 m within a halfspace for moment magnitude 3.0 at a hypocentral distance of 5 km.

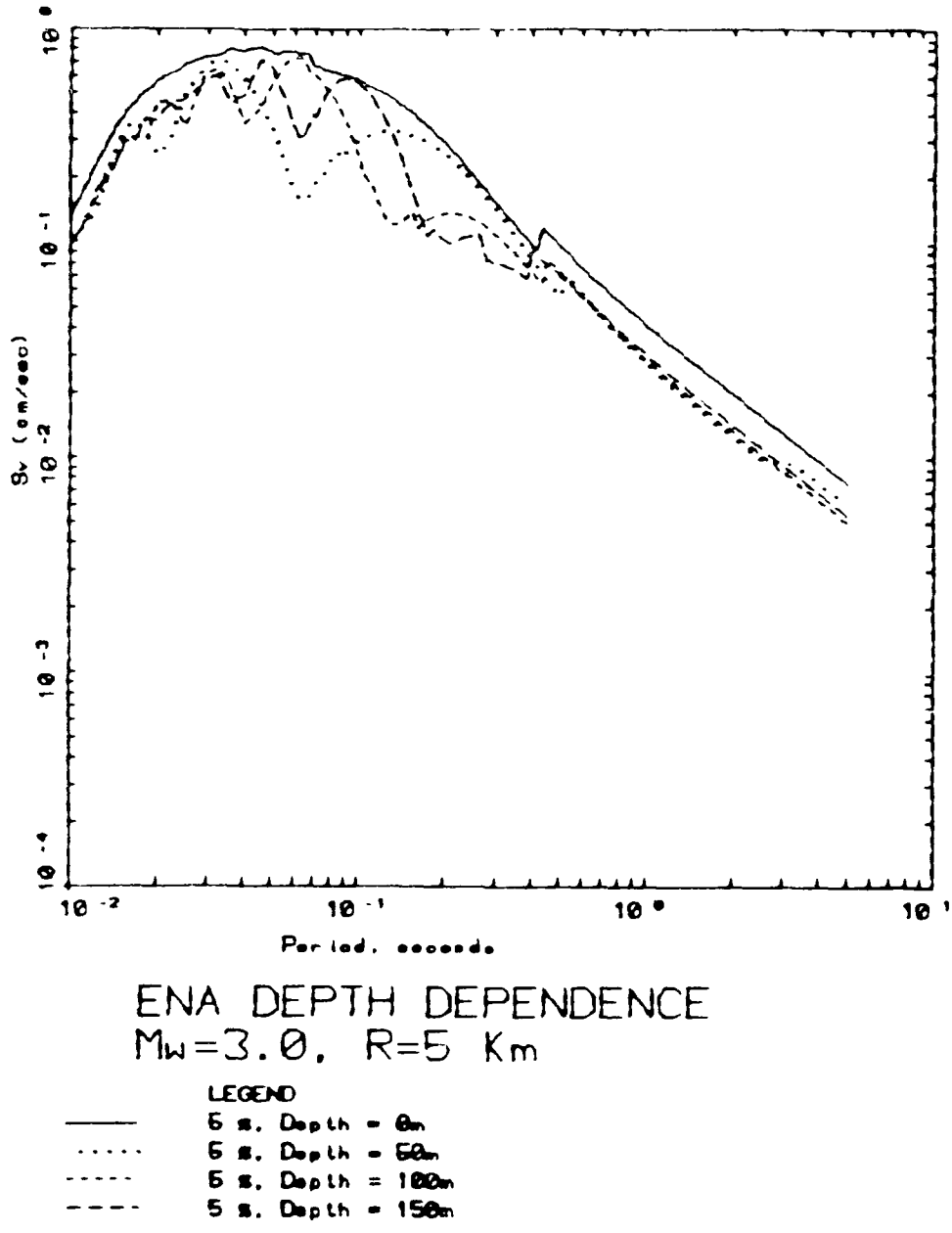

Figure 38 - Individual response spectra at the surface and at depths of 50, 100, and 150 m within a halfspace for moment magnitude 3.0 at a hypocentral distance of 5 km.

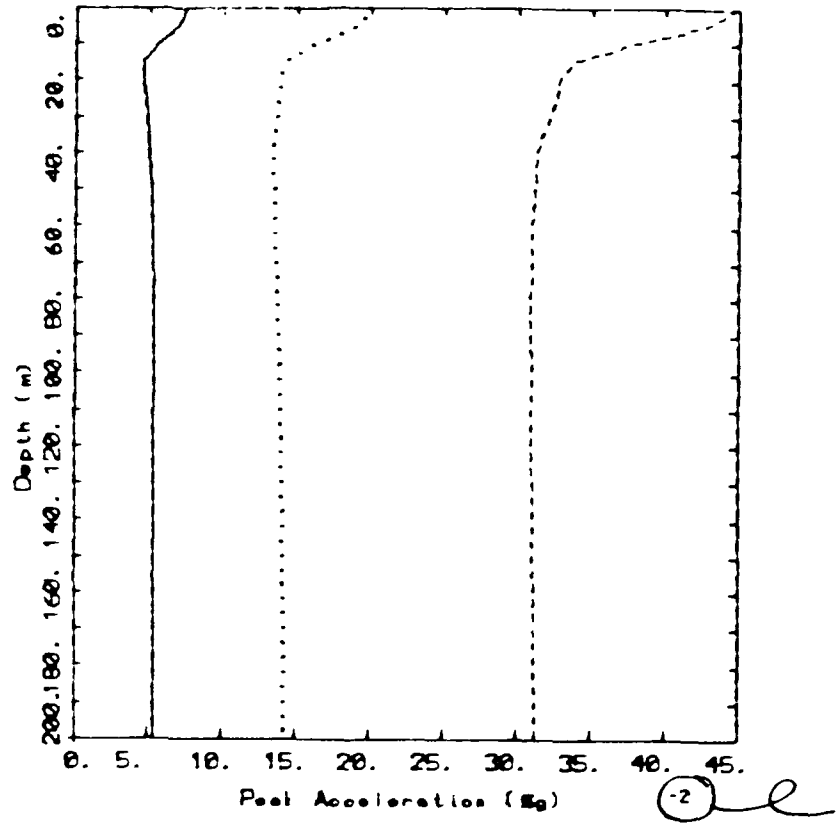

Figure 39 - WES-RASCAL predictions of peak ground acceleration as a function of depth in a halfspace. Peak ground acceleration for moment magnitudes 3, 4, and 5 at a hypocentral distance of 5 km are shown.

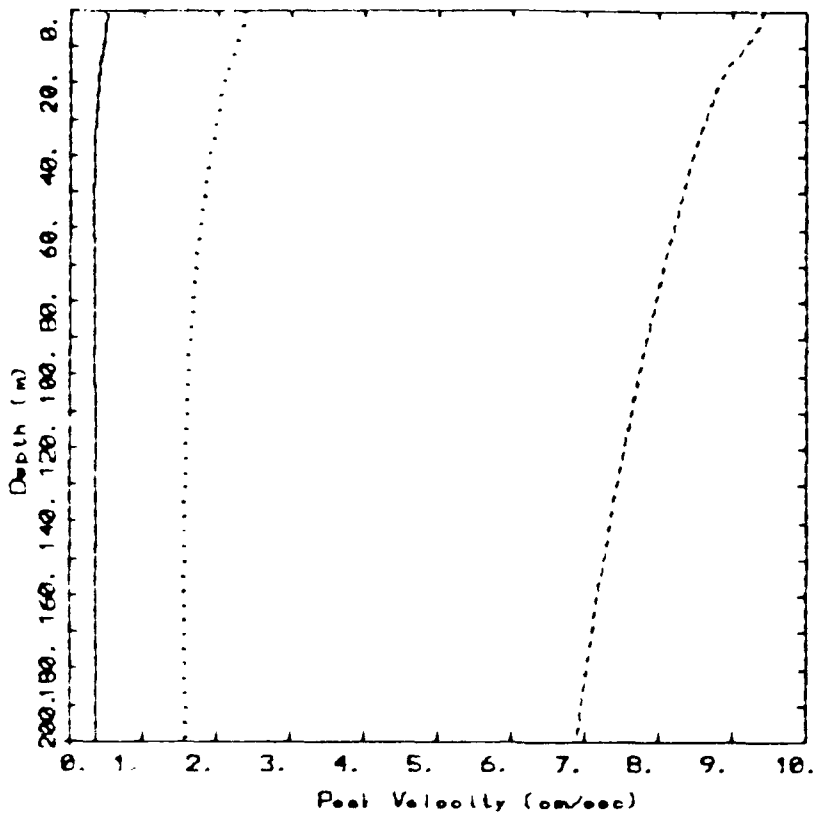

Figure 40 - WES-RASCAL predictions of peak ground velocity as a function of depth in a halfspace. Peak ground velocity for moment magnitudes 3, 4, and 5 at a hypocentral distance of 5 km are shown.